Effects of monomer composition on the electro-optic performance of polymer-stabilized blue phase liquid crystals

Von der Fakultät für Naturwissenschaften

der Universität Paderborn

genehmigte

Dissertation

zur Erlangung des akademischen Grades

Doktor der Naturwissenschaften

– Dr. rer. nat. –

von

Gaby Nordendorf, M. Sc.

Paderborn 2015

Die vorliegende Arbeit entstand im Zeitraum von April 2012 bis Juli 2015 im Fachgebiet für Physikalische Chemie an der Fakultät für Naturwissenschaften der Universität Paderborn unter Anleitung von Prof. Heinz-Siegfried Kitzerow.

1. Gutachter: Prof. Dr. Heinz-Siegfried Kitzerow
2. Gutachter: Prof. Dr. Claudia Schmidt

Die Arbeit wurde eingereicht am: 17.07.2015
Tag der mündlichen Prüfung: 27.08.2015

Danksagung

An dieser Stelle möchte ich mich bei allen Menschen bedanken, die auf die ein oder andere Weise zum Gelingen dieser Arbeit beigetragen haben.

Herrn Prof. Kitzerow danke ich für die Möglichkeit an diesem interessanten Thema zu arbeiten. Seine stete Diskussionsbereitschaft und Unterstützung hat mich durch meine Zeit als Doktorandin begleitet und diese Arbeit erst ermöglicht.

Unseren Projektpartnern bei Merck Darmstadt danke ich für die gute Zusammenarbeit. Insbesondere Dr. David Wilkes danke ich für fruchtbare Diskussionen und konstruktive Kritik.

Frau Prof. Schmidt danke ich für die Übernahme des Korreferats.

Für die Durchführung der Photo-DSC Messungen danke ich Rita Egert-Thiesbohnenkamp und Andreas Hoischen. Die anschließenden Diskussionen der Ergebnisse mit Herrn Hoischen haben grundlegend zu meinem Verständnis der Methode beigetragen.

Jürgen Schmidtke danke ich für die fachliche und moralische Unterstützung.

Für die Finanzierung des Projektes und die Bereitstellung der verwendeten Substanzen und Testzellen bedanke ich mich bei der Firma Merck KGaA Darmstadt. Des Weiteren möchte ich mich bei der Patentabteilung für die zügige Freigabe von Publikationen bedanken.

Auch bei meinen anderen Kollegen in der physikalischen Chemie möchte ich mich für das gute Arbeitsklima und die vielen netten Gespräche bedanken.

Nicht zuletzt möchte ich meiner Familie für ihre langjährige Unterstützung danken. Besonders danke ich Tobias für seine Geduld und Unterstützung in den hektischen Phasen der Promotion.

Contents

List of Figures

List of Abbreviations

bcc	body-centered cubic
BP	blue phase
BPI	blue phase I
BPII	blue phase II
BPIII	blue phase III
BPRM-1	blue phase reactive monomer 1 (mesogenic mono-methacrylate)
BPRM-2	blue phase reactive monomer 2 (mesogenic di-acrylate)
DTC	double-twist cylinder
EHA	2-ethylhexyl acrylate
FFS	fringe-field switching
HDDA	1,6-hexanediol diacrylate
HDDMA	1,6-hexanediol dimethacrylate
HTP	helical twisting power
IPS	in-plane switching
IRG 651	2,2-dimethoxy-1,2-diphenylethan-1-one
Iso	isotropic phase
ITO	indium tin oxide
LC	liquid crystal
LCD	liquid crystal display
MBBA	N-(4-methoxybenzylidene)-4-butylaniline
MDA-PB-3	nematic liquid crystal mixture
N	nematic phase
N*	chiral nematic phase
PAA	para-azoxyanisole
photo-DSC	photo differential scanning calorimetry
PMT	photo multiplier tube
POM	polarizing optical microscopy
PS-VA	polymer-stabilized vertical alignment
PSBP	polymer-stabilized blue phase

RM257	2-methylbenzene-1,4-diyl bis(4-[3-(acyloyloxy)propoxyl]benzoate)
RT	room temperature
sc	simple cubic
TFT	thin-film transistor
TN	twisted nematic
UV	ultra violet
VA	vertical alignment
VFS	vertical-field switching

1. Introduction

Liquid crystals (LCs) have unique electro-optic properties. The ability to modulate light by electrical addressing of the material is used in liquid crystal displays (LCDs). However, new liquid crystalline materials are needed to meet the criteria of advanced display technologies. One promising candidate for the next generation of display technology are polymer-stabilized blue phase (PSBP) liquid crystals.

Blue phases (BPs) are special liquid crystalline phases, which have probably been observed already in the 19^{th} century, but were seriously considered for applications not before the 21^{th} century. In 1888, Friedrich Reinitzer observed blue colors in cholesterol derivatives [1]. At that time, the nature of this colorful phenomenon was still unclear, but already the liquid state of the substance and its deviation from usual liquids were recognized. About twenty years later, Otto Lehmann introduced the term 'liquid crystal' for the state of matter observed by Reinitzer [2]. It took additional eighty years until the structure of blue phases was finally characterized. In memory of its first observation, it was given the name blue phase. However, the color depends on the periodicity of the BP structure and is not necessarily blue. Vivid research on BPs was conducted in the 1980s. The basic properties of BPs, such as phase sequence, structure and electro-optic behavior were studied [3]. At that time, BPs were only of academic interest, because of their narrow temperature range of existence. Applications became feasible more recently, when methods [4–8] were developed, which allow broadening of the BP temperature range. The most promising materials seem to be polymer-stabilized blue phases. During the last ten years, the topic of PSBP has been continuously studied. Basic understanding of underlying processes has been established and different approaches to improve the electro-optic characteristics have been presented.

Today, flat-panel displays are used in a wide range of applications including television, computer monitors and mobile phones. Nevertheless, there is still a demand for further improvements. For unrestricted use of LC devices in office, home or outdoor environments, a bright screen with wide viewing angle and high

contrast ratio is required. Other developments like 3D movies and color sequential displays require higher frame rates, for which fast switching of the LC is a precondition. In color sequential displays, color filters are redundant. Additionally, no white back-light is needed, which allows direct sequential control of red, green and blue light. This may reduce power consumption. For large-size TV screens, fabrication of high quality displays becomes a challenge. A simplified production process, where alignment layers are unnecessary, could help to reduce defects and costs at the same time. In general, displays need to become faster and cheaper in fabrication. Also reduced power consumption is attractive for transportable devices. In order to make these developments possible, new liquid crystalline materials with improved physical properties are required.

Polymer-stabilized blue phase liquid crystals meet some of the requirements listed for display applications. They allow extremely fast switching based on the Kerr effect and provide an optically isotropic dark state, when no voltage is applied, which saves energy. Because of the optically isotropic structure of BPs, no alignment layers are needed and production costs can be reduced. So far, high operation voltage, hysteresis and residual birefringence prevent the application of PSBP in devices.

To overcome these obstacles, chemical and technological concepts should be considered. From the point of view of a chemist, synthesis of new LC materials with improved properties is a key factor to enhance the performance. Modifying the composition of the BP mixtures is another possibility. On the technological side, design of new device is a logical route to improvement. Each of these factors has its own potential for optimization. However, combining them is essential to reach the best performance.

In this thesis, the electro-optic performance of a new type of PSBPs is investigated. To create the stabilizing polymer network, the mesogenic mono-functional monomer BPRM-1 (blue phase reactive monomer 1) is co-polymerized with one of the non-mesogenic cross-linkers BPRM-2 (blue phase reactive monomer 2), 1,6-hexanediol diacrylate (HDDA) or 1,6-hexanediol dimethacrylate (HDDMA). This is in contrast to studies of other groups [5, 9], where non-mesogenic mono-functional monomers were combined with mesogenic cross-linkers such as 2-ethylhexyl acrylate (EHA) and 2-methylbenzene-1,4-diyl bis(4-[3-(acyloyloxy)propoxyl]benzoate) (RM257), respectively. To our knowledge, it is the first time that mesogenic mono-functional monomers and non-mesogenic cross-linkers are used in PSBPs.

In this study, a deeper understanding of BP optics in the respective system should be established. Further more, interdependencies of sample composition and electro-optic performance of PSBPs are investigated with the aim to optimize the performance.

This thesis is organized as follows: In chapter 2, the theoretical background on optical and electrical properties of BPs is presented as well as basic LCD technologies. In addition, polymerization reactions are shortly introduced and the issue of polymer-stabilization of BPs is addressed. In chapter 3, the substances are described along with the preparation of test cells. Additionally, the analytical methods and their application are described. The results are discussed in chapter 4. General differences between unpolymerized and polymerized BP samples are addressed first. Then the results of systematic studies are presented including variations of sample composition and preparation conditions. Finally, conclusions are drawn and an outlook on further studies is given (chapter 5).

2. Background

The first liquid crystalline substances investigated were cholesteryl compounds. N-(4-methoxybenzylidene)-4-butylaniline (MBBA) and para-azoxyanisole (PAA) were also intensively studied. The breakthrough for commercial application of LCs was the synthesis of stable cynaobiphenyl and cyanotherphenyl compounds by George Gray and coworkers [10]. The response times of LCDs could be improved with the invention of cyano-phenyl cyclohexanes [11]. Other milestones in the history of LCs were the synthesis of fluorinated compounds, which have high dipole moments similar to nitrile compounds but lower rotational viscosity, and the development of nematic compounds with negative dielectric anisotropy, which are used for displays with vertical alignment (VA) mode. As a result of intense research, today, LC industry sells liquid crystalline compounds and LC mixtures optimized for specific applications.

Detailed explanations of LC related terminology and relevant optical and electrical properties with focus on BPs are given in sections 2.1 and 2.2. Basic LCD technologies are presented in section 2.3. In addition, the concept of free radical polymerization is described in section 2.4. In section 2.5, the combination of LCs and polymer networks to create PSBPs is addressed.

2.1. Some liquid crystalline phases and their optical properties

The BP structure is deduced from the basic nematic liquid crystal in section 2.1.1 and section 2.1.2 addresses the optical properties of nematic, chiral nematic and blue phase liquid crystals.

2.1.1. Blue phases: distinguished mesophases

Liquid crystals are ordered fluids. Among the large variety of LCs (fig. 2.1), this work is focused on thermotropic, calamitic LCs with high chirality. Thermotropic LCs consist of anisometric (e.g. rod-like or disc-like) molecules and form ordered

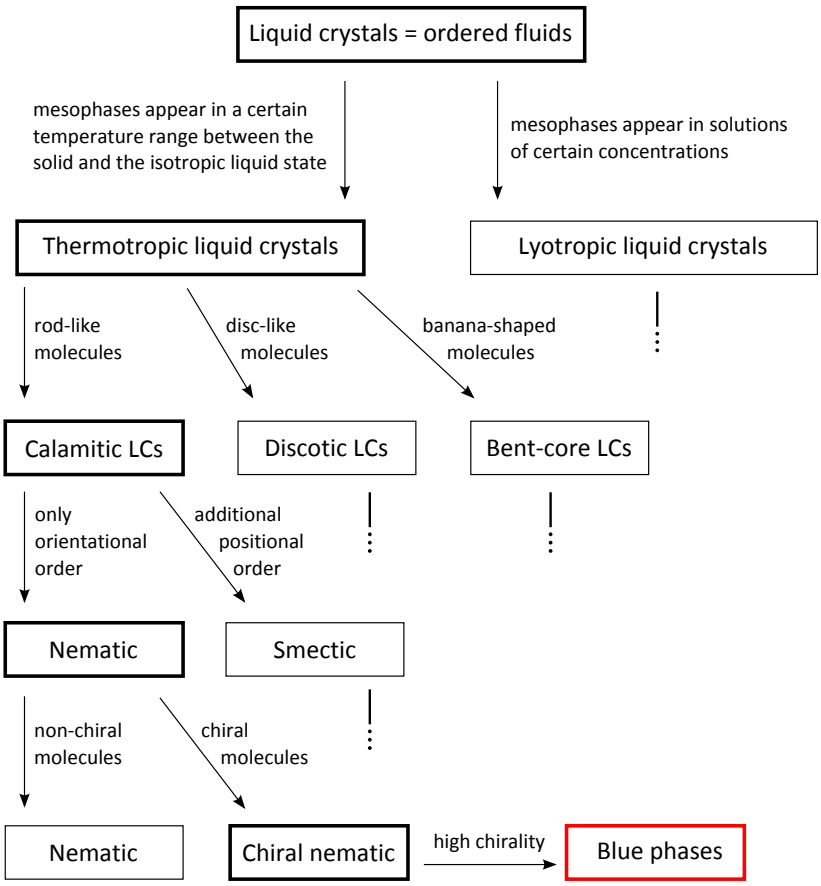

Figure 2.1.: Classification of some liquid crystalline mesophases. BPs are typically formed by thermotropic calamitic highly chiral nematic LCs. For references to the rather special cases of lyotropic BP, discotic BP, bent-core BP or smectic BP, see ref.[12].

fluid phases (mesophases) in a certain temperature range between the crystalline solid (fig. 2.2a) and the isotropic liquid phase (fig. 2.2c). With increasing temperature, the degree of order in the mesophases decreases. Thermotropic LC molecules (mesogenic molecules) typically combine a rigid moiety with flexible parts, which is essential for the appearance of mesophases.

The well-known nematic phase (N) of non-chiral mesogenic molecules is characterized by long-range orientational order only (fig. 2.2b) and can be described by the director $\vec{n}$, which describes the average molecular orientation in a small volume and may depend on position. As the director orientations $\vec{n}$ and $-\vec{n}$ are physically identical, the director is a pseudo vector with $|\vec{n}| = 1$.

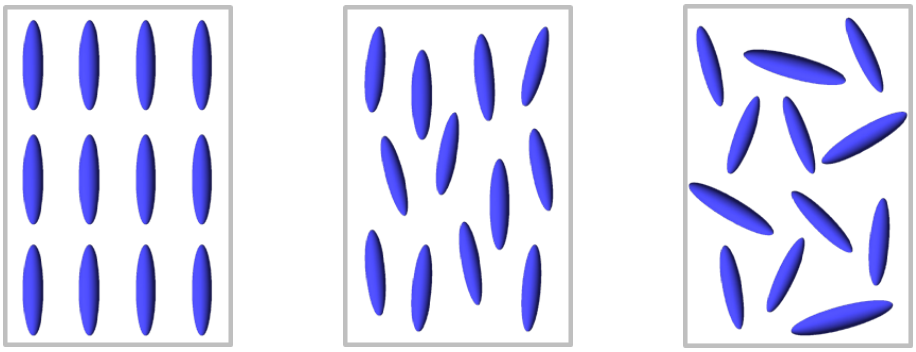

(a) solid crystal **(b)** nematic LC **(c)** isotropic liquid

Figure 2.2.: Liquid crystalline mesophases exist between the crystalline solid (a) and the isotropic liquid state (c). As representative of the meosphases, the nematic phase (b) of calamitic molecules, exhibiting long-range orientational order, is shown.

When chiral molecules are added to the nematic phase, twist is induced resulting in the chiral nematic phase (N^*). The latter is also called cholesteric phase. In chiral phases, the helical pitch p is the distance along the helical axis, over which the director orientation changes by 360° (fig. 2.3). For small pitch, twist along one single helical axis becomes disadvantageous and a double-twist structure forms [13]. In the center of a double-twist cylinder (DTC) (fig. 2.4a) molecules are oriented along the cylinder axis. Radial to the cylinder axis, molecules are twisted along countless helical axes.

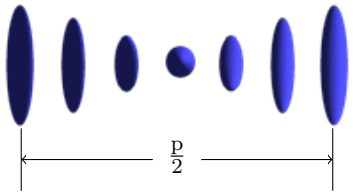

Figure 2.3.: Helical structure of the chiral nematic phase. A 180° rotation of the director is shown, which is equal to half the cholesteric pitch.

The double-twist structure is typical for the blue phase. Originating from the cylinder axis, the radial twist of the molecules is limited to 45° at the cylinder surface, which allows continuous changes of the director at the contact points of DTCs [13]. Thus, the diameter δ of a double-twist cylinder corresponds to one quarter pitch. When DTCs are packed in a cubic lattice, defects occur in

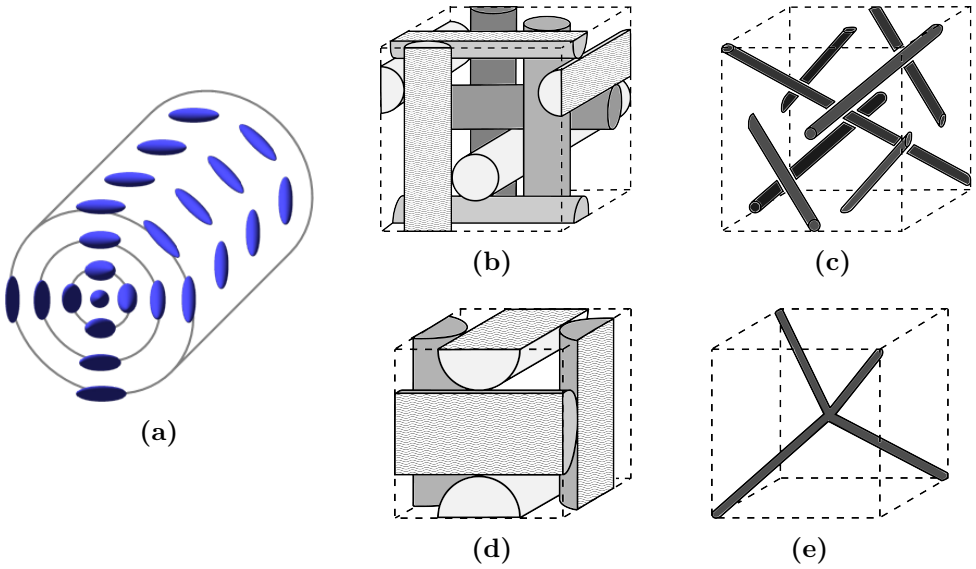

Figure 2.4.: Blue phase structure: The double-twist cylinder (a) as a basic structure is arranged in unit cells with different symmetries, body-centered cubic for BPI (b) and simple cubic for BPII (d). Discontinuities in the change of molecular orientations occur in the space between three double-twist cylinders. These disclinations are shown for BPI (c) and BPII (d), respectively. Adapted from ref. [14].

the space between three neighboring DTCs, where the director does not change continuously. In the core of these so-called disclination lines all orientational order is lost. In fig. 2.4, cubic unit cells and disclination lines are shown for the body-centered cubic (bcc) (figs. 2.4b and 2.4c) and simple cubic (sc) (figs. 2.4d and 2.4e) structures called blue phase I (BPI) and blue phase II (BPII), respectively. The lattice constant a of the unit cell is related to the pitch as follows: in BPI the relation is given by $a = 4\delta \approx p$ and in blue phase II (BPII) it is $a = 2\delta \approx p/2$ (compare figs. 2.4b and 2.4d, respectively). Apart from BPI and BPII, a third BP modification is known. Blue phase III (BPIII) has no cubic symmetry, instead the DTCs are randomly distributed without long-range order [3]. Because of the defect structure, BPs typically exist in a small temperature range (<1 K) between the chiral nematic and the isotropic phase (Iso).

2.1.2. Optical properties of N, N* and BP

As shown in section 2.1.1, the order varies for different mesophases. Consequently, their optical properties differ as well.

The nematic phase is uniaxially birefringent and the optical axis coincides with the director. Linearly polarized light is affected by different refractive indices depending on the plane of polarization, which is the plane spanned out by the electric field vector and the propagation direction of the wave. The refractive indices are called extraordinary refractive index n_e and ordinary refractive index n_o for polarizations parallel and perpendicular to the director, respectively. The birefringence

$$\Delta n = n_\mathrm{e} - n_\mathrm{o} \tag{2.1}$$

of a nematic liquid crystal is given by the difference of the extraordinary and the ordinary refractive index.

Another optical effect is observed in N* with well ordered helices, which often show bright colors resulting from selective reflections: Circularly polarized Bragg reflections due to the chiral periodic order of the liquid crystal. Bragg reflections occur in materials with periodic lattices, when the Bragg condition

$$m\lambda = 2d\sin\theta \tag{2.2}$$

is satisfied, with wavelength of the incident beam λ, $m \in \mathbb{N}$, distance of the lattice planes d and angle of incidence θ (fig. 2.5). In chiral nematic LCs the distance of the lattice planes coincides with half the helical pitch. For normal incidence, only first order reflections are allowed ($m = 1$), but for oblique incidence higher order reflections may be observed. Circularly polarized light of the same handedness as the helix is reflected in a bandwidth $\Delta\lambda = p\Delta n$ around the Bragg wavelength $\lambda_\mathrm{Bragg} = p \cdot \bar{n}_{N^*}$ with an averaged refractive index

$$\bar{n}_{N^*} = \sqrt{\frac{1}{2}n_\mathrm{e}^2 + \frac{1}{2}n_\mathrm{o}^2}, \tag{2.3}$$

where n_e and n_o are the refractive indices of the corresponding untwisted nematic phase [15].

Blue phases are optically isotropic and show no birefringence. However, they are locally anisotropic in volumes which are small compared to the unit cell. In blue phases Bragg scattering can be observed. BPs may show several selective

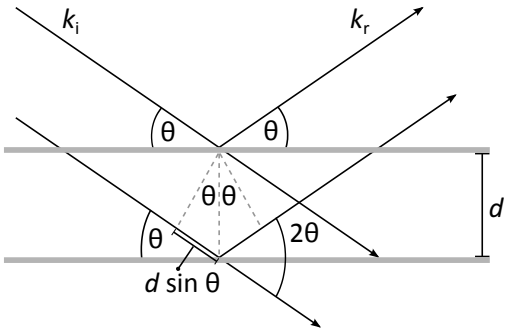

Figure 2.5.: Incident light with parallel wave vectors k_i is reflected k_r at different lattice planes. For phase retardations equal to $2d\sin\theta$ the reflected wavelengths interfere constructively and Bragg reflections are observed.

reflections. The Bragg wavelengths

$$\lambda_{Bragg} = \frac{2a \cdot \bar{n}_{BP} \cdot \sin\theta}{(h^2 + k^2 + l^2)^{1/2}} \tag{2.4}$$

with the averaged refractive index

$$\bar{n}_{BP} = \sqrt{\frac{1}{3}n_\mathrm{e}^2 + \frac{2}{3}n_\mathrm{o}^2} \tag{2.5}$$

depend on the orientation of the lattice planes with respect to the incident beam, where (h, k, l) are the Miller indices of a set of planes. Possible combinations of the Miller indices depend on the BP symmetry. In simple cubic symmetry all h, k, l are allowed, while in body-centered cubic systems the sum $h + k + l$ needs to be even [16]. Based on the selection rules for Bragg reflections in blue phases [17] the lattice planes can be assigned to the different reflection wavelengths. The ratio of adjacent reflection wavelengths is $1/\sqrt{2}$, $1/\sqrt{3}$, $1/\sqrt{4}$, ... in BPI and BPII [18]. For normal light incidence ($\theta = \pi/2$), Bragg reflections observed for BPs are circularly polarized [19].

Different liquid crystalline phases show characteristic temperature dependences of Bragg reflections. For N^*, BPI and BPII, the typical temperature dependence of the selective reflections is shown in fig. 2.6. Phase transitions are indicated by discontinuous changes of the Bragg wavelengths. Notably, BPI can be supercooled. Therefore when cooling the sample, BPI reflections may be visible at temperatures where N^* exists when it is heated. The reflections of N^* and BPII weakly depend on temperature, while the reflections of BPI are blue-shifted with

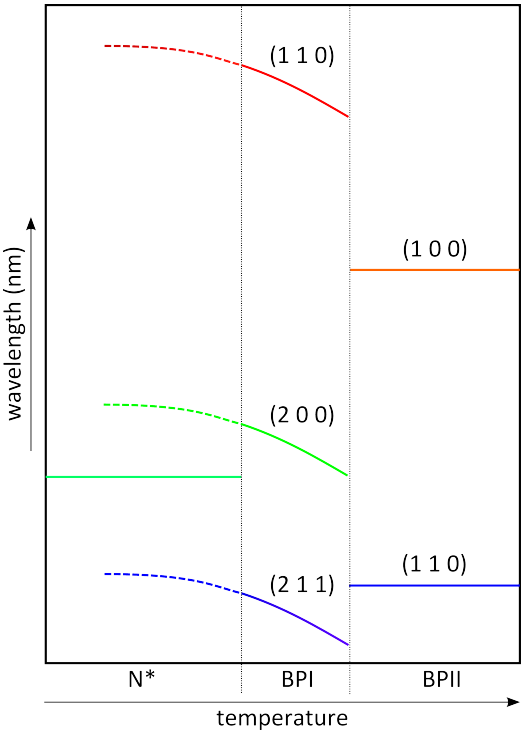

Figure 2.6.: Typical temperature dependence of Bragg reflections in N^*, BPI and BPII (solid lines). BPI is supercooled (dashed lines) to temperatures, where normally N^* exists. Adapted from ref. [16].

increasing temperature. This continuous change results from contraction of the BP lattice. The lattice planes in fig. 2.6 have been assigned according to eq. (2.4) and the selection rules for bcc structure in BPI [16, 17] and for sc structure in BPII.

The periodic lattices of BPI and BPII with a lattice constant of a few 100 nm can provide selective reflections in the visible wavelength range. When cubic BPs are investigated with polarizing optical microscopy (POM), typically a platelet texture is observed (fig. 2.7). Grain boundaries separate areas with different lattice orientations, represented by platelets of different colors. The thermal conditions during platelet growth influence the size of the platelets. When the temperature is changed slowly, growth of large areas with uniform alignment is promoted.

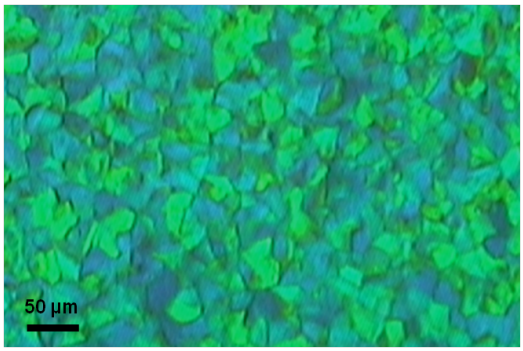

Figure 2.7.: Typical platelet texture of a cubic BP observed by POM. Different wavelengths are reflected, depending on the orientation of the lattice with respect to the incident light.

2.2. Electric field effects

The electric field exerts forces on the BP structure owing to the local dielectric anisotropy of the liquid crystal. With increasing electric field strength the following effects can be observed: Kerr effect, electrostriction and field-induced phase transitions. The Kerr effect results from local director reorientations, while electrostriction and field-induced phase transitions are accompanied by changes of the BP lattice. The effects are described in more detail in sections 2.2.1 to 2.2.3.

2.2.1. Electro-optic Kerr effect

The anisotropy of the molecular shape leads to anisotropic dielectric properties. The dielectric displacement induced by an electric field parallel and perpendicular to the director is expressed by the constants $\epsilon_{\parallel}$ and $\epsilon_{\perp}$, respectively. Dependent on the local dielectric anisotropy

$$\Delta\epsilon = \epsilon_{\parallel} - \epsilon_{\perp}, \tag{2.6}$$

the molecules align parallel or perpendicular to the electric field for $\Delta\epsilon > 0$ and $\Delta\epsilon < 0$, respectively. This molecular reorientation in an electric field results in a change of birefringence, which is referred to as Kerr effect. The Kerr effect is a quadratic electro-optic effect. In spite of their local anisotropy, blue phases show no macroscopic birefringence because of their cubic structure. For weak electric fields, the induced birefringence Δn_{ind} in BPs is approximately proportional to

the square of the electric field E

$$\Delta n_{\mathrm{ind}} = K\lambda E^2. \tag{2.7}$$

The Kerr constant K is the proportionality factor depending on the probe wavelength λ. For high electric fields, the Kerr effect is described by an extended Kerr model [20]

$$\Delta n_{\mathrm{ind}} = \Delta n_{\mathrm{sat}} \left(1 - \exp\left[-\left(\frac{E}{E_{\mathrm{sat}}}\right)^2\right]\right), \tag{2.8}$$

with a characteristic field strength E_{sat}. In the limit of high electric field, the induced birefringence saturates reaching the value Δn_{sat}. Using a series expansion, the extended Kerr model can be reduced to the simple eq. (2.7) for low electric fields. The Kerr constant depends on material properties of the LC such as local refractive index anisotropy Δn, dielectric anisotropy $\Delta\epsilon$ and the average elastic constant K_{el} as well as the pitch p. According to Gerber [21], the Kerr constant is related to these properties by

$$K = \Delta n_{\mathrm{sat}} \cdot \Delta\epsilon \frac{\epsilon_0 \cdot p^2}{K_{\mathrm{el}} \cdot \lambda \cdot (2\pi)^2}. \tag{2.9}$$

A high Kerr constant can be obtained by using materials with large Δn, large $\Delta\epsilon$ and large p. However, improving these properties is limited by trade-offs [15], e.g. a pitch in the visible wavelength range reduces the contrast ratio and increases the response time. The response time is also increased for highly viscous materials with large $\Delta\epsilon$ [22].

The dynamic behavior of the Kerr effect is another important aspect. The relaxation of the molecules, when the voltage is switched off, is described by the decay time t_{off}, which may be approximated as [23]

$$t_{\mathrm{off}} \approx \frac{\gamma_1 \cdot p^2}{K_{\mathrm{el}} \cdot (2\pi)^2}, \tag{2.10}$$

where γ_1 is the rotational viscosity of the LC material. While the decay time is independent of the applied voltage, the rise time t_{on} depends on the applied voltage as follows [24]

$$t_{\mathrm{on}} = \frac{t_{\mathrm{off}}}{(\frac{V}{V_c})^2 - 1}, \tag{2.11}$$

where V_c is the critical voltage for unwinding the pitch. Additionally to the local reorientation of molecules described above, the response time is affected by a second process, which is slower and results from lattice deformations [25].

In this work, the Kerr constant is derived from voltage dependent transmittance measurements (for details see section 3.3.2) as depicted in fig. 2.8. Three

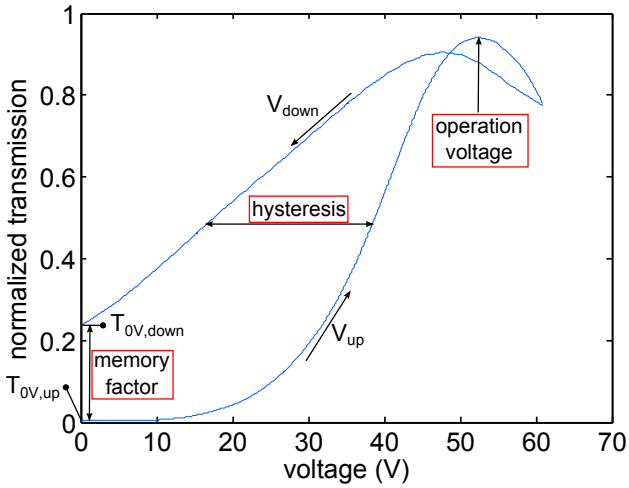

Figure 2.8.: Definition of important parameters for electro-optic performance.

additional quantities can be extracted from the voltage-transmittance curves: operation voltage V_{op}, hysteresis ΔV and residual birefringence. The latter may be expressed in form of a memory factor M.

Figure 2.8 shows the field-induced transmittance of a BP sample placed between crossed polarizers. The voltage corresponding to the first transmittance maximum is called operation voltage V_{op}. Applying the operation voltage allows switching between the dark and the bright state of the cell. Gray-scale control is achieved applying intermediate voltages. The operation voltage is proportional to $1/\sqrt{K}$ [20, 22].

The hysteresis ΔV specifies the difference between the voltages at the half height of the maximum transmittance (fig. 2.8) measured for increasing ($V_{\uparrow,50\%}$) and decreasing ($V_{\downarrow,50\%}$) voltage:

$$\Delta V = V_{\uparrow,50\%} - V_{\downarrow,50\%}. \tag{2.12}$$

As hysteresis affects the accuracy of gray-scale control, it is undesired for display applications. Hysteresis depends on the maximum voltage applied to the cell: ΔV

becomes considerably larger for $V > V_{\mathrm{op}}$ and can be reduced applying $V < V_{\mathrm{op}}$. Unfortunately, for $V < V_{\mathrm{op}}$ the contrast ratio is reduced simultaneously.

Residual birefringence at the end of a voltage cycle reduces the contrast ratio. To measure the amount of residual birefringence, the memory factor

$$M = \frac{T_{\downarrow,0V}}{T_{\uparrow,0V}} \tag{2.13}$$

is defined, where $T_{\uparrow,0V}$ and $T_{\downarrow,0V}$ are the transmittances at the beginning and the end of one voltage cycle, respectively. When voltage is applied and removed several times, residual birefringence may alter the starting point of the next cycle. Thus, the contrast ratio of the device is reduced further with every additional voltage application.

2.2.2. Electrostriction

In intermediate electric fields, the cubic BP lattice is continuously distorted. This distortion, known as electrostriction, results in continuous changes of the selective reflection wavelengths. A red-shift of Bragg reflections indicates increasing spacing of the corresponding lattice planes, while decreasing lattice spacings result in blue-shifted reflection wavelengths. Whether the lattice is compressed or dilated in the direction of the electric field depends on the local dielectric anisotropy of the LC and the direction of the electric field with respect to the symmetry axes of the BP lattice. The deformed unit cells become tetragonal, trigonal or orthorombic, when the electric field is parallel to a fourfold, threefold or twofold axis, respectively [26]. In materials with $\Delta\epsilon > 0$ for most BP lattice orientations a red-shift of the reflection wavelengths is observed in direction of the electric field, but some BPI lattice orientations show blue-shifted reflections, which is referred to as anomalous electrostriction [27]. When the lattice is dilated in direction of the electric field for LCs with $\Delta\epsilon > 0$, compression would be observed in LCs with $\Delta\epsilon < 0$ for the same lattice plane.

2.2.3. Field-induced phase transitions

Different kinds of field-induced phase transitions have been found to appear when the cubic BP is subjected to an external electric field: the cubic BP can change into tetragonal [28, 29] or hexagonal BPs [30–32] as well as into N^*, and for very high field strengths changes from N^* to N (helical unwinding) were observed [27,

33]. The symmetry of the resulting phases appearing for increasing field strength is gradually reduced and the BP to BP transitions may additionally affect the orientation and faceting of the platelets.

2.3. Liquid crystal displays

As discussed in sections 2.1 and 2.2, the electro-optical properties of LCs enable modulation of light. This concept is used to build LCDs. The breakthrough in LCD technology was the invention of the twisted nematic (TN) cell in 1971 by Schadt and Helfrich [34]. This cell type enabled fabrication of flat-panel displays for transportable devices such as calculators and digital watches, because of its low power consumption. Over the years, the technology has been further improved and LCDs with higher information content have been produced [35]. Another milestone of LCD technology was the invention of active matrix displays, where each pixel is attached to a transistor and a capacitor. This allows switching of single pixels, while the state of other pixels is actively maintained by the connected capacitors. In the course of the developments, other display technologies such as vertical alignment (VA) mode and in-plane switching (IPS) mode were invented, which provide an excellent viewing angle. Both technologies are mainly used in TV applications. VA mode is used in particularly large displays.

The basic element of LCDs are cells made of a pair of parallel glass substrates filled with LCs in between. The nematic molecules are aligned by an orientation layer. An applied electric field modifies the orientation of the LCs. In one of the states the cell appears bright and in the other one it appears dark. Gradually changing voltages allow gray-scale control. For specific switching modes, the orientation of the LC molecules, the switching behavior and the geometry of the transparent electrodes differs.

In the following sections 2.3.1 to 2.3.3, the basic functionality of three common LCD technologies (TN, VA and IPS mode) is presented. Subsequently, the cell design for blue phase liquid crystals is addressed in section 2.3.4.

2.3.1. TN mode

In twisted nematic (TN) mode displays, orientation layers induce planar alignment of the nematic LC along a preferred axis. The orientation of this preferred axis differs by 90° between the two alignment layers. This forces, in the ground state, the nematic liquid crystal to twist inside the cell as shown in fig. 2.9a. This display

mode is named after the twisted arrangement of the nematic molecules. The linear polarizers at the outer side of the glass substrates are oriented in such a way that the plane of polarization coincides with the director at the respective LC interface. The plane of polarization of linearly polarized light is rotated by 90° within the cell and can pass the second polarizer. Consequently, the cell appears bright in the ground state.

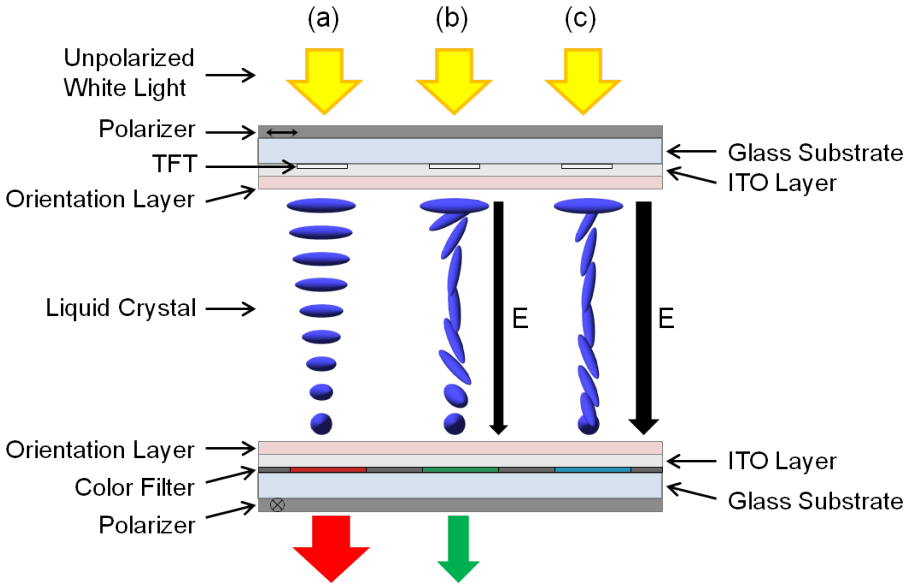

Figure 2.9.: Configuration of a TN mode display and orientation of the nematic molecules when (a) no electric field, (b) a small electric field or (c) a large electric field is applied.

The glass substrates are coated with transparent indium tin oxide (ITO) electrodes on the inner side of the cell. When an electric field is applied to the cell, the nematic molecules tilt vertically to the substrate, because LCs with positive dielectric anisotropy align parallel to the electric field. At the boundary to the orientation layer the planar alignment remains, if the anchoring strength of the orientation layer is sufficiently high. The situation for small electric fields is depicted in fig. 2.9b. Starting from the boundary, where the molecules are still aligned in a planar way, a continuous tilt vertical to the substrates is induced. However, the twisted symmetry of the ground state is not completely eliminated so that some light can still pass the second polarizer. A small transmittance occurs. When the field strength is further increased the regime of large electric fields is reached. The molecules, which are not forced into a planar state by boundary conditions,

align vertically to the substrates and no twist symmetry remains. This is shown in fig. 2.9c. The plane of the incident linearly polarized light is no longer rotated, and therefore the light is absorbed by the second polarizer. The cell appears dark.

In the TN cell, a homogeneous electric field in the direction vertical to the substrates is produced by ITO electrodes coated on the glass substrates. Such a cell geometry is referred to as vertical-field switching (VFS) cell. The working principle of the TN cell results not from this general cell design but from the specific orientation of the nematic molecules induced by the orientation layers. The basic cell design is modified to build LCDs. Generally, thin-film transistors (TFTs) are added to supply the necessary voltage and color filters in red, green and blue are used in the pixels to enable mixing of all desired colors. Gray-scale control is provided by the LC. As the LC material itself does not emit light, an additional backlight is needed for display applications.

TN technology offers very fast response times and low power consumption as nearly no current flows in the cell. However, a directional backlight and demanding phase compensation are needed to obtain a wide viewing angle.

2.3.2. VA mode

Vertical alignment (VA) mode displays use a different alignment than TN cells. The orientation layer induces homeotropic alignment of the LC molecules. This means that in the ground state the LC director is oriented vertical to the substrate (fig. 2.10). The light can not pass the crossed polarizers so that the ground state of a VA display is dark.

For VA technology the same VFS geometry of the cell is used as in TN cells. However, the switching mechanism is different. VA cells are filled with nematic LCs with negative dielectric anisotropy. Consequently, the molecules preferentially align perpendicular to the electric field. As shown in fig. 2.10, this leads to a continuous change of the director orientation: Starting from the boundary, where the molecules are anchored in vertical position by the orientation layer, the molecules tilt and align parallel to the substrates in the middle of the cell. The light incident on the LC layer is linearly polarized. The plane of polarization is oriented in an angle of 45° with respect to the tilt direction of the LC. When it passes through the LC, the initially linear polarization is changed to an elliptical polarization. Only the part of the elliptically polarized light that oscillates in the same plane of polarization as the second polarizer is transmitted. The cell appears bright.

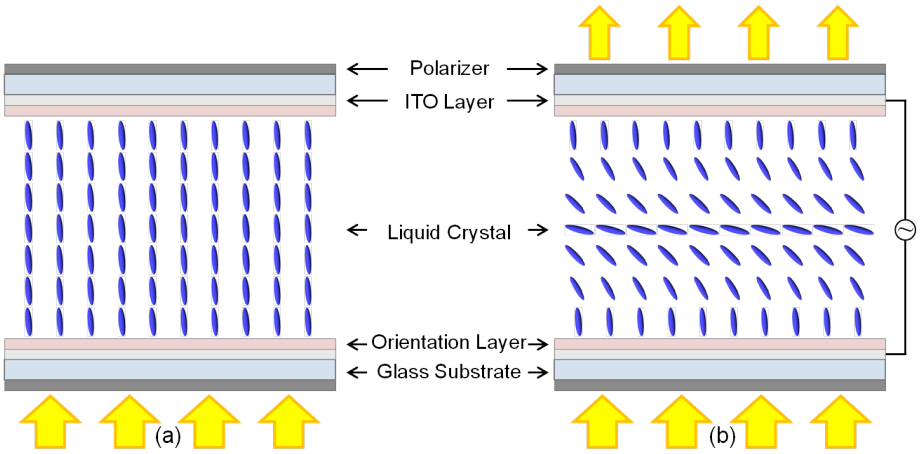

Figure 2.10.: Configuration of a VA mode display (a) without an electric field and (b) reorientations of the molecules in the electric field.

In comparison with TN technology, the transmittance in VA displays is reduced and the response times are slower. At the same time, a better dark state, higher contrast ratio and a wider viewing angle are realized in VA technology. Based on VA mode, polymer-stabilized vertical alignment (PS-VA) mode was developed, where the director is fixed with a slight tilt angle by polymerization instead of being homeotropically aligned. This uniform pretilt of the molecules enforces switching in a specific direction, when an electric field is applied.[36]

2.3.3. IPS mode

In contrast to the display technologies described above, the in-plane switching (IPS) mode applies an electric field in the film plane. To realize this in-plane field, comb-like interdigitating electrodes are located on one glass substrate (bottom substrate) as depicted in fig. 2.11.

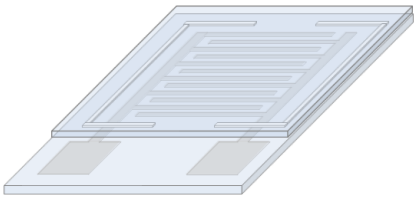

Figure 2.11.: In-plane switching cell with interdigitating electrodes on the bottom substrate.

Simulated field distributions indicate high field strength near the electrode edges and a reduced field strength in the center between adjacent electrodes [37]. The profile of the field distribution and the penetration depth of the electric field can be influenced by width and spacing of the electrodes [38, 39]. In general, the electro-optical performance in IPS cells is independent of the cell thickness as long as the penetration depth of the electric field is smaller than the cell thickness.

In IPS mode displays, planar alignment is induced by orientation layers. These layers promote an axis of preferred orientation parallel to the long-axis of the electrode strips. Consequently, the nematic LC aligns planar on the substrate with the director pointing along the electrode strips in the ground state (fig. 2.12a). The crossed polarizers are oriented in such a way that the plane of polarization of the second polarizer is parallel to the director. When linearly polarized light is incident on the nematic molecules, the plane of polarization is unaffected and the light is absorbed by the second polarizer. The cell appears dark in the ground state.

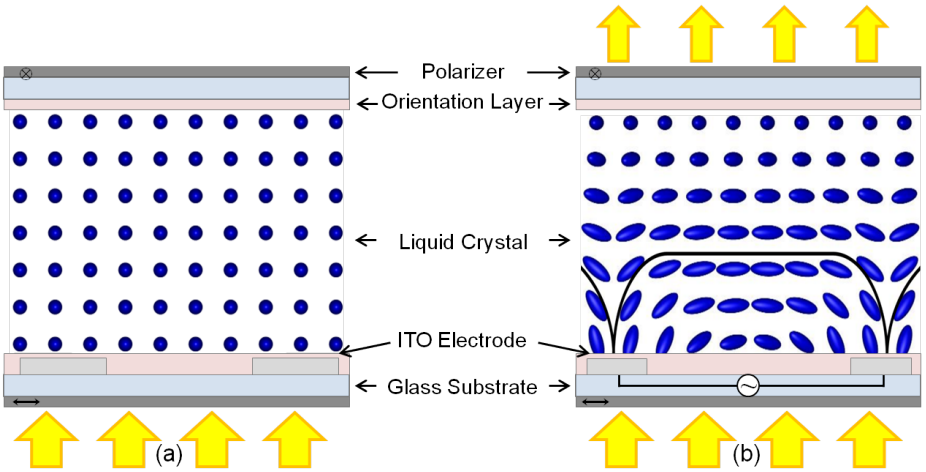

Figure 2.12.: Configuration of an IPS mode display (a) without an electric field and (b) reorientation of the molecules in the electric field.

Application of an electric field results in reorientation of the nematic molecules in the plane. LCs with positive dielectric anisotropy are used, which align preferentially parallel to the electric field. The field distribution in IPS cells is inhomogeneous (fig. 2.13): Above the electrode surfaces the vertical field component dominates, while the space between electrodes is dominated by the horizontal field component [38]. This also leads to different alignment of the molecules in both areas (fig. 2.12b). First, the arrangement between electrodes is discussed. Here,

the LC director is aligned parallel to the glass substrates by the electric field. This results in a twist of the nematic molecules similar to the ground state of TN cells. The plane of linearly polarized light incident on the LC layer is rotated and passes the second polarizer. The area between electrodes appears bright. Another situation is observed above the electrodes. Here, the molecules align almost vertically to the substrate. The linearly polarized light is absorbed by the crossed polarizer and the area above the electrodes appears dark.

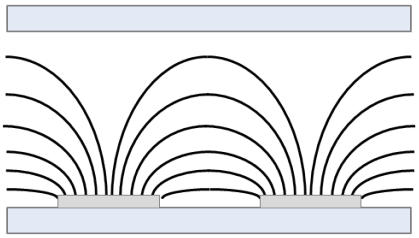

Figure 2.13.: Lines of force in an in-plane switching cell.

Using interdigitating electrodes has advantages as well as disadvantages. The inhomogeneous field in IPS mode displays results in a wide symmetrical viewing angle, which can be realized with simple biaxial compensation films [40]. Therefore, expensive compensation foils as used in standard TN displays are not needed. On the other hand, transmittance is reduced because only the areas between electrodes contribute and a brighter backlight than in TN mode is needed.

2.3.4. Cell design for blue phases

The three commonly used display modes presented in sections 2.3.1 to 2.3.3 are based on two cell types with VFS and IPS geometry, respectively. The same cell types are used to investigate BPs, which are considered for next generation display applications. However, only IPS has the potential to be used for displays, because the electric field needs to be parallel to the glass substrates to see the change in transmittance resulting from induced birefringence. A general advantage of using BPs with a cubic structure is that no alignment layers are needed. In this section, advantages and disadvantages of using the two cell geometries in combination with BPs are presented.

VFS cells can only be used for electro-optic measurements, when the light is incident on the cell at an oblique angle. Then, they offer low operation voltage, negligible hysteresis and fast response times because of the homogeneous field distribution. On the other hand, spectroscopic investigations at normal incidence

rely on VFS cells because the largest deformation of the BP unit cells appears in direction of the electric field for liquid crystals with positive dielectric anisotropy.

In a recent study it was discussed that the interaction of BP liquid crystals with the glass substrate differs from interactions with the electrode surface in IPS cells: Lan et al. [41] report that cubic BP unit cells arrange in elliptical tertiary structures above the electrode surface, which align parallel to the long-axis of the electrodes. This leads to non-ideal optical isotropy of the dark state and a reduced contrast ratio. Another drawback is the strong fringe field near the electrode edges, which causes local lattice distortions, thereby increasing hysteresis and response times [23]. As only horizontal field components contribute to the transmittance of the cell [38], IPS cells may have even lower transmittance than VFS cells under oblique light propagation. However, transmittance can be improved by using protrusion electrodes, which increase the penetration depth of the electric field. Optimizing the shape of the protrusion electrodes can further increase the horizontal field contribution [37].

In addition to these often used cell geometries, cells with different electrode configurations have been proposed. An overview of some cell configurations is given in ref. [12] including IPS geometry with protrusion electrodes and fringe-field switching (FFS) geometry.

2.4. Polymerization

The term polymerization describes the chemical reaction of monomers forming polymer chains or polymer networks. According to Flory [42], there are two types of polymerization reactions, step-growth and chain-growth polymerizations. This terminology describes the respective reaction process: in step-growth reactions, the polymerization proceeds step by step from monomer to oligomer and finally to polymer, while in chain-growth reactions one molecule after the other is added to the initiated polymer chain. Therefore, chain-growth reactions are also called addition reactions. Typical chain-growth reactions are free radical polymerization and ionic polymerization. Step-growth reactions are typically condensation reactions [43] and high conversion as well as high molecular weight of the polymer are reached only for long reaction times. In contrast, polymers of high molecular weight form almost immediately in chain-growth reactions, and with further reaction time only the total amount of polymer increases.[44]

In the following, the reaction mechanism of free radical polymerization, which is used in this study, is explained. Basically, the free radical polymerization is characterized by three steps:

1. Initiation: $\mathrm{I} \rightarrow \mathrm{I}^*$
   An active species is generated from an initiator (I).

2. Chain growth: $\mathrm{I}^* + \mathrm{M} \rightarrow \mathrm{IM}^* \xrightarrow{\mathrm{M}} \mathrm{IMM}^* \rightarrow \mathrm{IM}_i^*$
   The active species reacts with a monomer (M) and initiates chain growth. The active center is transferred to the end of the chain. More monomers add to the chain. The index i indicates the degree of polymerization.

3. Termination: $\mathrm{M}_i^* + \mathrm{M}_j^* \rightarrow \mathrm{M}_{i+j}$
   Two active polymer chains combine.

These steps are discussed in more detail in sections 2.4.1 to 2.4.3.

2.4.1. Initiation

The initiator is activated by an external stimulus, which can be thermal or photochemical. Photochemical initiation is based on light absorption. The best initiator efficiency is obtained, when the initiator is illuminated with light of the wavelength that matches its absorption maximum.

The photochemically initiated generation of an active species is explained for the photo-initiator 2,2-dimethoxy-1,2-diphenylethan-1-one (IRG 651), which is used in this study. The decomposition is shown in fig. 2.14. In a first step, the photo-initiator decomposes by α-cleavage (Norrish type I reaction) [45, 46]. The bond between carbonyl group and α-carbon atom breaks, which yields a benzoyl and a 2,2-methoxybenzyl radical. The latter decomposes by β-fission and a methyl radical as well as an inactive methyl benzoate are obtained. The formed radicals may react with each other, which results in further products [45]. Chain growth is most effectively initiated by the benzoyl radical formed by α-cleavage [47].

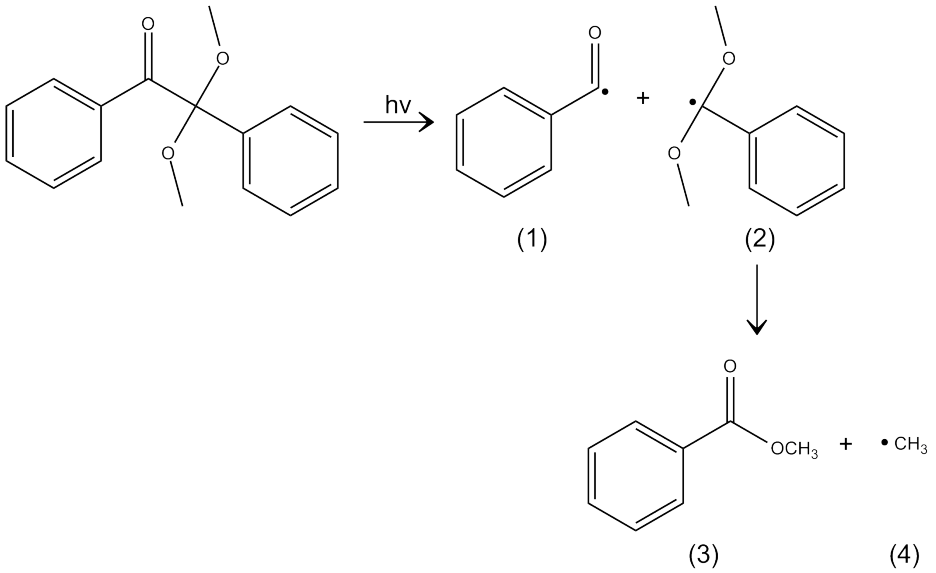

Figure 2.14.: Photo-induced decomposition of the photo-initiator Irgacure 651 by α-cleavage. Two radicals, a benzoyl radical (1) and a 2,2-methoxybenzyl radical (2), are obtained. By sequential β-fission of (2) the inactive methyl benzoate (3) and a methyl radical (4) are formed.

2.4.2. Chain growth

The initiator radical, formed in the first step, reacts with a monomer and thus starts the chain growth. Subsequently, more and more monomers add to the active chain. In the simple case that only one monomer species is present, this is called homopolymerization. When two different monomers react with each other, it is called copolymerization. For copolymerization, four possible reaction mechanisms exist:

1. The active chain with the end group M_1 reacts with monomer M_1.
   $\sim M_1 \cdot + M_1 \xrightarrow{k_{11}} \sim M_1 M_1 \cdot$

2. The active chain with the end group M_1 reacts with monomer M_2.
   $\sim M_1 \cdot + M_2 \xrightarrow{k_{12}} \sim M_1 M_2 \cdot$

3. The active chain with the end group M_2 reacts with monomer M_1.
   $\sim M_2 \cdot + M_1 \xrightarrow{k_{21}} \sim M_2 M_1 \cdot$

4. The active chain with the end group M_2 reacts with monomer M_2.
   $\sim M_2 \cdot + M_2 \xrightarrow{k_{22}} \sim M_2 M_2 \cdot$

The probability for these reactions to occur is related to the reactivity ratios

$$r_1 = \frac{k_{11}}{k_{12}} \quad \text{and} \quad r_2 = \frac{k_{22}}{k_{21}},$$

where k_{11}, k_{12}, k_{22} and k_{21} are the reaction constants of the respective reactions. A reactivity ratio $r_1 > 1$ indicates that the monomer M_1 preferentially reacts with itself, and a reactivity ratio $r_1 < 1$ indicates that reactions with the monomer M_2 are preferred. When the reactivity ratio of both monomer types is larger than one, block-copolymers with long units of one species are formed. However, this constellation is very rare.[44]

In free radical polymerization, the reactive sites of the monomer are typically double-bonds. The number of the functional groups within one molecule determines the degree of cross-linking in the polymer. One reactive group leads to chain growth. Two or more reactive groups enable cross-linking. The density of the polymer network increases with the number of functional groups. With increasing amount of polymer, the viscosity of the system increases and the reaction rate decreases. When mono-functional and di- or multi-functional groups are copolymerized, the structure of the polymer network also depends on the reactivity ratio of the monomers.

2.4.3. Termination

Deactivation of radicals terminates the chain growth. Typically, two radicals are involved in this termination step. For free radical polymerization, two competitive termination mechanisms are known:

1. Combination: $M_i\cdot + \cdot M_j \rightarrow M_{i+j}$
2. Disproportionation: $M_{(i-2)}\text{-}CH_2\text{-}XHC\cdot + \cdot CHX\text{-}CH_2\text{-}M_{(j-2)} \rightarrow$
   $M_{(i-2)}\text{-}CH_2\text{-}CH_2X + XHC{=}CH\text{-}M_{(j-2)}$

Whether one of the mechanisms dominates, depends on the used monomers. Products from combination reactions have higher molecular weight than the active chains. If disproportionation occurs, changes in weight are negligible. In addition, a reactive group results from disproportionation, which can be activated by a free radical and restart chain growth. This leads to branched or cross-linked polymers.

In bulk polymerization of monomers with more than one functional group, additional effects such as the Trommsdorff effect and vitrification may occur; in free radical polymerization, a highly cross-linked polymer network forms in an early

stage of the reaction. The system becomes highly viscous and the reaction is controlled by diffusion. This leads to a reduced rate of termination reactions, because diffusion of large polymers with active centers is hindered. At the same time, forming initiator-radicals can still start new polymer chains. The initiation rate becomes larger than the termination rate and the reaction is autoaccelerated. This effect is called Trommsdorff or gel-effect [48]. With increasing conversion the viscosity of the system further increases. At some point also diffusion of small units is hindered and a glass-like state is formed [49].

2.5. Stabilization of the blue phase

Typically, BPs exist in a very narrow temperature range close to the clearing point of the chiral LC. This temperature needs to be considerably broadened for applications. Considering display applications, the operating temperature range required for indoor applications is 0 °C to 50 °C and for mobile and automotive applications the required range is even larger −20 °C to 70 °C and −40 °C to 100 °C, respectively [15].

In the last years, different possibilities to stabilize the BP and thereby enlarging the temperature range have been demonstrated. Unconventional shapes of the nematic host molecules, such as dimer [7] or bent-core [6, 50–52] molecules, as well as hydrogen-bonding [53] can cause larger BP temperature intervals. In another approach, the BP was doped by short polymers [54] or nanoparticles [8, 55–59], which also resulted in a larger temperature range because the defect structure was stabilized. A third possibility is polymerization. In 1993, Kitzerow et al. [4] polymerized the LC molecules forming a glass like state. While it was possible to get stable BP over a wide temperature range, electrical addressing was impeded by the cross-linked network. Consequently, this technique could not be used for electro-optic switching. In 2002, Kikuchi's group [5] reported a wide temperature-range BP (over 60 K) stabilized by a gel-like polymer network, which became known as polymer-stabilized blue phase (PSBP). The electro-optical properties of the LC are preserved in PSBPs. For that reason, PSBPs are of major interest for display applications. More details on PSBPs and optimizing their performance are given in section 2.5.1 and section 2.5.2, respectively.

2.5.1. Polymer-stabilized blue phase

A multi component system is necessary to form a polymer-stabilized blue phase. Such a system used for polymer stabilization contains a nematic LC, a chiral dopant, mono- and di- or tri-functional monomers and a photo-initiator [5]. The components and their function in the polymerization process are described in detail in section 3.1.

In PSBPs, the BP structure is stabilized by a polymer network. This polymer network is formed by in-situ photo-polymerization of monomers. Careful choice of the reactive monomers and suitable concentrations are needed to create a switchable gel-like state. The photo-polymerization is initiated by ultra violet (UV) light of defined intensity, to which the sample is exposed for a certain time. During the polymerization process, the polymer separates from the LC and assembles in the disclination lines [60, 61]. As a result, a gel-like composite of polymer and LC is generated. Thus, the polymer network stabilizes the defect structure and the BP temperature range is expanded towards lower temperatures, where normally N^* would be stable [15]. This method preserves the properties of the LC such as fast response times, because of the phase separation of polymer and LC. However, the operation voltage increases in PSBP compared to pure BPs without monomers [62]. Furthermore, hysteresis and residual birefringence occur.

2.5.2. Optimizing the electro-optic performance of PSBP

High operation voltage, hysteresis and residual birefringence of PSBP are the major problems for applications. There are two completely different strategies to optimize the electro-optic performance: Either designing new devices as mentioned in section 2.3.4 or improving the BP system. The latter can be realized by synthesizing new LCs with high Kerr constant. Besides, changes of the sample composition also offer possibilities for optimization. Since optimization of one factor might deteriorate an other, it is necessary to always consider the whole system and the interactions of different factors. Trade-offs cannot be completely avoided.

From common BP mixtures [5, 63], it is known that the Kerr constant decreases with increasing temperature [20]. In general, a large Kerr constant is beneficial to obtain a low operation voltage. Therefore, it is important to start with a high Kerr constant in the BP system. This can be achieved by using a smaller amount of chiral dopant, since the Kerr constant becomes higher when the lattice constant increases [64, 65]. On the other hand, shifting the Bragg reflections out of the UV

wavelength range typically reduces the contrast ratio and the response time [22, 23] making the material useless for display applications. Another possibility to get a high Kerr constant in the PSBP is a weak polymer network [65], which in turn results in slower response times [23]. Additionally, a weak polymer network is less stable and may be deformed more easily when an electric field is applied, so that hysteresis and residual birefringence are increased [65, 66]. Even rupture of a weak polymer network needs to be considered. In other words, a weak polymer network is no reasonable option to optimize the electro-optic performance.

The stability of the polymer network is influenced by the monomer composition and by the polymerization conditions. Considering the monomer composition, one can change the total monomer fraction as well as the ratio of mono- and di-functional monomers. A larger monomer fraction increases the stiffness of the polymer network as does a higher cross-linking density. However, the amount of polymer is limited by the volume of disclinations to ensure phase separation while stabilizing the BP structure. As mentioned before, the resulting increase of the operation voltage can not be avoided, but other parameters like hysteresis and response times are improved. For photo-polymerization the exposure time as well as the intensity and the wavelength of the UV light can be adapted. The curing conditions specify the homogeneity of the formed polymer network in the cell. Accordingly, IPS cells should be illuminated from the side without electrodes, especially if the electrodes are opaque. The polymerization starts at the illuminated side (top substrate). In order to get a homogeneous polymer network throughout the cell, it is important to initiate the polymerization near the bottom substrate as soon as possible. Hence, the wavelength chosen for illumination needs to penetrate the cell completely and absorption by LC molecules and already formed polymer needs to be minimized [67]. A slower polymerization rate can help to reduce the absorption. A uniform polymer network also reduces hysteresis [67]. According to Xu et al. [68], polymerizing with linearly polarized UV light can further enhance response times and hysteresis, when the polarization axis, along which the stronger polymer network forms, is oriented perpendicular to the interdigitated electrodes.

3. Experiments

In this chapter, the substances we worked with are shortly presented (section 3.1). Additionally, sample preparation and experimental methods are described. Section 3.2 is divided in two parts: mixture preparation and processing and preparation of the test cells, which includes polymer-stabilization. As experimental methods POM, spectroscopy, electro-optic characterization and photo differential scanning calorimetry (photo-DSC) were used. Experimental setup, measurement techniques and analysis for the optical methods are described in section 3.3. The photo-DSC technique is described in section 3.4.

3.1. Materials

According to Kikuchi's findings [5], the following compounds are necessary for the successful creation of PSBPs: a nematic LC, a chiral dopant, a mono-functional and a di-functional monomer and a photo-initiator. For this work, such substances were provided by Merck KGaA (Darmstadt, Germany). While Kikuchi and the majority of other scientists used a non-mesogenic mono-functional monomer and a mesogenic di-functional cross-linker, the aim of the present study is exploring the opportunities of using a mesogenic mono-functional monomer and a non-mesogenic cross-linker. A more detailed explanation regarding the different compounds is given in sections 3.1.1 to 3.1.4. The test cells are described in section 3.1.5.

3.1.1. Nematic liquid crystal

The nematic liquid crystal is often referred to as the host because it is the main component of the BP mixture. Combining different nematic molecules might be favorable to optimize the properties of the LC host, for example to lower the melting point, thereby expanding the temperature range of the nematic phase. Properties of the nematic host highly influence the performance of the BP system. To meet the criteria for applications, high thermal stability and photo resistivity are preconditions. The high temperature limit of the BP mixture is given by the

clearing point T_c of the LC host, which is reduced by adding the other components of the BP mixture.

The nematic LC mixture MDA-PB-3 was used throughout this work. It is stable for a long time period and has a large dielectric anisotropy $\Delta\epsilon > 120$ at 25 °C. The clearing temperature of the nematic host is 74 °C.

3.1.2. Chiral dopant

Chiral dopants are molecules that induce chirality in a non-chiral liquid crystal. This leads to the appearance of induced cholesteric (N^*) phases and even BPs, if the helical pitch becomes sufficiently small. The ability to induce a helical structure in a non-chiral medium can be described by the helical twisting power (HTP). The HTP value depends mainly on the chiral dopant, but also on the LC host. For small mass fractions χ_w of the chiral dopant, the reciprocal value of the pitch is approximately proportional to χ_w, $p^{-1} = \mathrm{HTP} \cdot \chi_w$, where $\mathrm{HTP} = \lim_{\chi_w \to 0}(p \cdot \chi_w)^{-1}$. However, the mass fraction of chiral dopant that is soluble in the host is limited. Hence, compatibility of both components is important to achieve good results.

In this study, R5011 (fig. 3.1) with $\mathrm{HTP} > 150\,\mu\mathrm{m}^{-1}$ was used [69]. Because of its high HTP, small amounts of the chiral dopant were sufficient to induce BPs. When doping the nematic host with 2.8 % R5011, the induced BP showed selective reflections in the visible wavelength range. Only a slightly higher amount of 3.8 % R5011 shifted the selective reflections of the BP into the UV range [70]. Reflections in the UV range are a prerequisite for display applications, while visible Bragg reflections are helpful for the fundamental investigation of underlying processes.

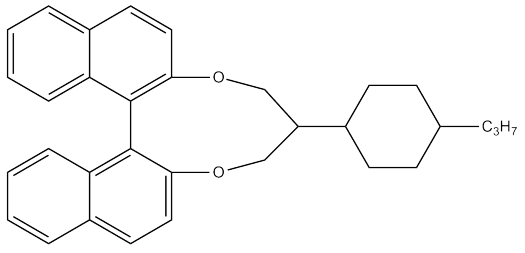

Figure 3.1.: Chemical structure of the chiral dopant R5011.

3.1.3. Monomers

Monomers with different functionality are used to create cross-linked polymer networks. The mono-functional monomers ensure chain propagation, while the di-functional monomers control the cross-linking density of the polymer network. The stiffness of the polymer network is influenced by the mesh width. A narrow meshed network (high cross-linking density) is more rigid than a wide meshed network.

The monomers can be classified as monomers with and without mesogenic units. The structure of mesogenic monomers and LC molecules is similar. Hence, mesogenic monomeres have a good solubility in LCs and the clearing point T_c is only slightly reduced, when mesogenic monomers are added to LCs. In contrast, non-mesogenic monomers are less soluble in LCs, which results in aggregation of the monomers and separation from the LC, especially at high concentrations. Additionally, the clearing point T_c is largely reduced by adding non-mesogenic molecules to the LC. The higher the concentration of non-mesogenic monomers, the lower T_c becomes. This reduction only affects unpolymerized samples. Complete polymerization raises the value to the clearing point of the chiral nematic host, which is lower after polymerization than in the original mixture. This change of the clearing temperature directly results from polymerization: For a mixture containing initially 10 wt% monomers and 3.8 wt% chiral dopant, the fraction of chiral dopant increases to 4.2 wt%, when the monomers are completely polymerized, because it is dissolved in a smaller fraction of liquid compounds. It is known that T_c is lower in mixtures with higher chirality. If T_c remains below the value expected for the host, this may be an indicator for incomplete polymerization.

In this work, combinations of the mono-functional mesogen BPRM-1 with three different cross-linkers have been investigated. The studied cross-linkers were the mesogenic di-acrylate BPRM-2 and the two non-mesogenic compounds HDDA and HDDMA (fig. 3.2). The electro-optic performance of PSBP made from mixtures containing HDDA or HDDMA, respectively, was compared.

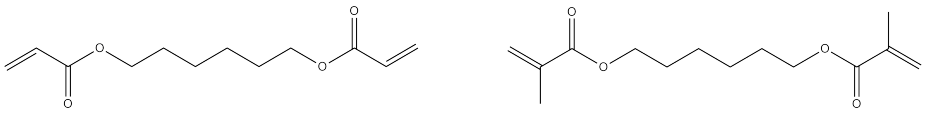

(a) HDDA **(b)** HDDMA

Figure 3.2.: Chemical structures of the non-mesogenic cross-linkers.

3.1.4. Photo-initiator

The photo-initiator IRG 651 (fig. 3.3) is used in this study. The colorless, crystalline compound has a local absorption maximum at about 340 nm and the strongest absorption is reached below 300 nm [71]. For activation, a UV light source with a broad emission spectrum (300 nm to 570 nm) and maximum intensity at about 360 nm is used [72]. As shown in section 2.4.1, the initiator decomposes by α-fission.

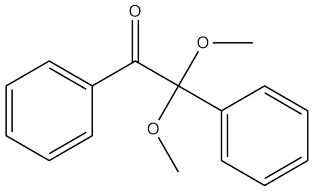

Figure 3.3.: Chemical structure of the photo-initiator IRG 651.

3.1.5. Test cells

Two different types of test cells were used in this work (fig. 3.4). Both cell types have electrodes made of ITO, which is transparent in the visible wavelength range.

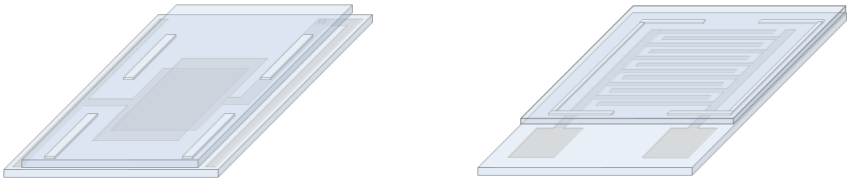

(a) VFS cell **(b)** IPS cell

Figure 3.4.: Two different types of test cells have been used for the experiments.

The cells used for VFS (fig. 3.4a) are commercially available from E.H.C Co. (Tokyo, Japan). The cell type KSSZ-10/A111P1NSS consists of two glass substrates with ITO electrodes and a polyimide coating, which are separated by 10 µm spacers. The electrode area is 10 mm × 10 mm and the polyimide layer induces planar alignment of the LC without a preferred orientation of the molecular long axis (degenerated planar).

IPS cells (fig. 3.4b) have comb-like electrodes on the bottom substrate and were covered with a glass substrate without electrode. The cell thickness d is 10 µm. In this work, IPS cells with ITO electrodes with an electrode width w and an electrode spacing s with $w = s = 10$ µm were used. The substrates are not treated with any alignment layer. These cells were provided by Merck KGaA.

3.2. Sample preparation

In this section, a general preparation procedure is described. For particular investigations, the preparation may differ from this general procedure. The exact sample compositions for the different studies are listed in appendix A and respective references are given in the corresponding sections in chapter 4.

3.2.1. Mixture preparation and processing

Blue phase mixtures were prepared from the nematic liquid crystal mixture MDA-PB-3 and the chiral dopant R5011. To enable polymer stabilization, the monofunctional mesogen blue phase reactive monomer 1 (mesogenic mono-methacrylate) (BPRM-1) and a di-functional cross-linker (HDDA, HDDMA or BPRM-2) were added, together with the photo-initiator IRG 651. Similar BP systems have been investigated in ref. [73], where the focus was on the improvement of the components and their compatibility.

A small stirring bar (Micro 0.8 cm × 0.3 cm, VWR) was added to a brown glass vial (Rotilabo-short thread ND8 vials, volume 1.5 ml, Carl Roth GmbH + Co. KG). The different components were added by weight, starting with the liquid compounds (cross-linker, LC host) using a syringe. The viscous LC host was heated to 85 °C, thereby changing to the less viscous isotropic phase, before adding it to the mixture. Then the solid compounds (R5011, BPRM-1) were added. The last compound added to the mixture was the crystalline photo-initiator, of which only a very small amount was needed. The typically required amount of 0.2 mg was added directly to the mixture standing on the analytical balance (Mettler Toledo

AG245) with a precision of 0.01 mg. If the weight of a portion added is below the sensitivity of the analytical balance, deviations from the desired concentration may occur. Even though the mixtures were carefully prepared, it was not always possible to avoid this. The vials were closed with a matching screw cap (screw cap, closed, PP, ND9, Sept. Silik./PTFE, Carl Roth GmbH + Co. KG).

The mixtures were sensitive to UV irradiation and therefore handled under yellow light conditions to avoid unintended polymerization. The prepared mixtures were stirred for at least 10 min at 85 °C at about 300 rpm for homogenization (MR Hei-Standard with EKT Hei-Con temperature controler, Heidolph).

3.2.2. Preparation of test cells

The test cell was placed on the hot-stage and filled at 85 °C with the homogenized mixture. A droplet of the isotropic mixture was placed next to the cover glass so that it could flow into the cell gap driven by capillary forces. To support the formation of a uniform blue phase, the sample was heated up to the isotropic phase and cooled down to 20 °C. This procedure was repeated twice. To determine the phase sequence, the temperature was increased in intervals of 0.2 K in the interesting temperature range.

For polymer stabilization, the test cell was cooled down from the isotropic state to a temperature 0.5 K above the N^* to BP transition. It was exposed to UV irradiation (10 min, 3 mW cm^{-2}) of a high pressure mercury lamp (Hönle bluepoint 4) while keeping the temperature constant. Subsequently, the sample was cooled to room temperature (RT) to check BP stability.

3.3. Electro-optic measurements

In this work, different kinds of electro-optic investigations have been performed, measurement of Bragg reflections (section 3.3.1), investigation of the Kerr effect (section 3.3.2) and dynamic switching experiments (section 3.3.3). Before describing the different methods, a general description of the setup and common preparation steps is given.

The measurement setup (fig. 3.5) was based on a Leitz Ortholux II Pol-BK polarization microscope with halogen lamps, which can be used to measure either in transmission or reflection mode. If not mentioned otherwise, polarizer and analyzer were crossed. The microscope possesses two standard eyepieces and a camera mount. The camera (JVC, TK-C1380E) was adjusted at an azimuthal angle of

45° with respect to the crossed polarizers. The camera's field of view was shown on the computer monitor. The two tubes of the standard eyepieces were used to add a photo multiplier tube (PMT) detector (Hamamatsu, R 6925) and a fiber spectrometer (Ocean Optics, USB 2000+ UV–VIS–ES) with a spectral resolution of 1.5 nm. The PMT detector was operating at 600 V supplied by a high voltage supply (Ortec, model 556). A hot-stage, which was built in house, was fixed on a rotatable table. This hot-stage enables temperature control between 0 °C and 100 °C with an accuracy of 0.01 K. The square wave (1 kHz) was either generated by a waveform generator (Wavetek, model 270) or by the computer sound card and amplified by a factor of 100 (Krohn-Hite, model 7500). An oscilloscope (PicoScope, 2203) registered the voltage applied to the test cells. Reported voltages are defined as amplitude from 0 to peak. The applied voltage is limited to 200 V in this setup.

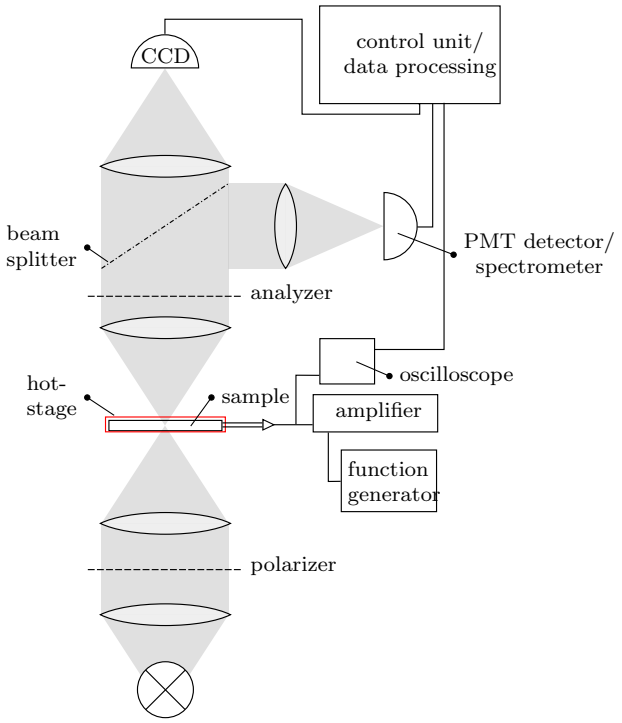

Figure 3.5.: Schematic drawing of the electro-optic setup.

The test cell was aligned on the hot-stage. The rotatable table was adjusted to an azimuthal angle of 45° between the long-axis of the test cell and the crossed polarizers. If the investigated sample was filled in an IPS cell and heated to the

isotropic phase, the ITO electrodes became visible and the camera was used to orient the electrode strips at an angle of 45° with respect to the crossed polarizers. For VFS cells, the sample was first adjusted parallel to one of the polarizers, which corresponds to the darkest state. Subsequently the sample was rotated by 45° using the scale of the rotatable table. Adjusting the VFS cell in this way, became a habit when working with nematic LCs. It should not have any influence on the results, because of the cubic BP structure.

For temperature dependent measurements, the temperature was increased in steps of 0.2 K and 2 K for unpolymerized and polymerized samples, respectively. The temperature range chosen for unpolymerized samples started at the N^* to BP transition temperature and ended in the isotropic phase. Hence, the investigated temperature range changed from sample to sample, ranging typically between 4 K and 8 K. Polymer-stabilized samples were investigated from 20 °C to 60 °C. Consequently, the BP to isotropic transition was included into the measurement and the lower temperature limit was high enough so that no condensation of water droplets on the cell occurred.

The subsequent methods of investigation required varying measurement conditions, which are described in the following sections 3.3.1 to 3.3.3 together with the data analysis.

3.3.1. Measurement of Bragg reflections

For the first measurements of Bragg reflections (when the fiber spectrometer was not yet available) the camera was exchanged with a spectrometer (Oriel, Multispec combined with Instaspec IV), while the eyepieces could serve their original purpose. The Oriel spectrometer has a spectral range from 300 nm to 850 nm and a resolution of 0.5 nm.

Samples were prepared in VFS cells. Both temperature and voltage dependent measurements were performed in reflection mode. Before starting the investigation of the sample, a dark spectrum and a reference spectrum were measured with a mirror inside the beam path and with crossed and parallel polarizers, respectively. The sample was illuminated with white light from a halogen lamp. At each temperature, one spectrum was measured at zero voltage. Subsequently, the voltage was adjusted manually from 0 V to 100 V in steps of typically 1 V and checked on a multimeter (PeackTech 2010 DMM). The cells were addressed with a square wave at a frequency of 1 kHz. One spectrum was saved for each voltage. The same was done for decreasing voltage steps.

To obtain the final reflection spectrum, the dark spectrum was subtracted from the reference and the sample spectrum. Then, the reflection was calculated by dividing the sample spectrum by the reference spectrum. The resulting spectrum showed peaks at the reflected wavelengths. Peaks were fitted using the program Origin. A peak fitting algorithm with Gaussian shape was used as shown in fig. 3.6.

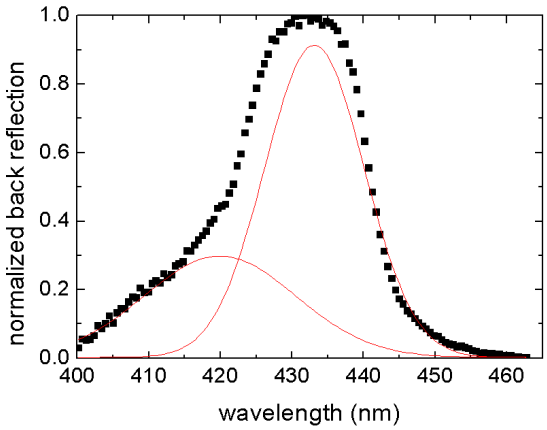

Figure 3.6.: Gaussian fit of two peaks for a normalized reflection spectrum of a pure BP at a distinct temperature.

With this spectrometer, Bragg reflections could only be measured for samples with visible selective reflections above approximately 350 nm, because of the absorption edge of the glass substrates. Dr. Jürgen Schmidtke prepared also cells from quartz glass and used the fiber spectrometer to investigate reflections in the UV range. However, a broad absorption band occurred in this region so that no additional information was obtained.

An important precondition for these spectroscopic studies was that the respective sample either contained no photo-sensitive substances or was already polymerized. Otherwise, the polymerization process might have been induced by the UV part of the irradiation from the halogen lamp, thereby inducing changes in the sample characteristics.

3.3.2. Static measurements

The static properties of the Kerr effect were characterized by measuring 4 important quantities: Kerr constant, operation voltage, hysteresis and memory factor (section 2.2.1).

For this purpose, IPS cells were investigated in transmission. A small band gap interference filter with a transmission maximum at 542 nm was used to restrict the spectral range of the white light source. With green light incident on the sample, also investigations of uncured samples containing photo-sensitive compounds were possible. For reasons of comparability, the same condition was applied to the polymerized samples.

The temperature dependent measurement was controlled by a LabVIEW routine. A triangular pulse of 1 ms multiplied with the square wave of 1 kHz was used for a voltage sweep including increasing and decreasing voltage (fig. 3.7). The voltage reached at the maximum of the pulse was set manually for the first measurement. For the following measurements, the transmittance maximum of the preceding measurement was calculated and the maximum voltage of the subsequent measurement was chosen to be 10 V above the last operation voltage. The data of 10 sweeps were averaged for each temperature. The data for all temperatures were analyzed with respect to Kerr constant, operation voltage, hysteresis and memory factor as described below.

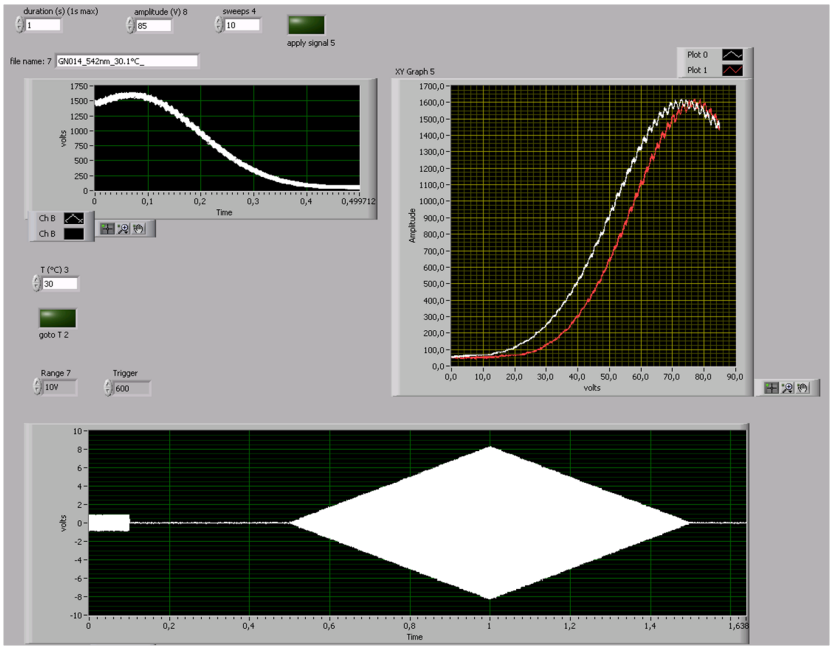

Figure 3.7.: View of a measurement routine used for static measurements at one temperature with input values and output graphs. The voltage-dependent transmittance is on the upper right side and the triangular pulse used for addressing is on the bottom. In a later version, measuring at different temperatures with constant intervals was enabled.

For the setup shown in fig. 3.5, the intensity of transmitted light is given by

$$I = I_{\max} \cdot \sin^2\left(\frac{\pi \cdot \Delta n_{\text{ind}} \cdot d}{\lambda}\right), \tag{3.1}$$

where $I_{\max}$ is the maximum value of transmitted light, Δn_{ind} is the field-induced birefringence and d is the cell thickness. With increasing voltage, the first transmittance maximum appears for $(\pi \Delta n_{\text{ind}} d)/\lambda = \pi/2$. The penetration depth of the electric field in the IPS cell is assumed to be equal to the cell thickness d. Further, a homogeneous field distribution $E = V/s$ is assumed. For the analysis eq. (3.1) was rearranged and Δn_{ind} was replaced according to eq. (2.7):

$$\begin{aligned}
\frac{I}{I_{\max}} = T &= \sin^2\left(\frac{\pi \cdot \Delta n_{\text{ind}} \cdot d}{\lambda}\right) \\
T &= \sin^2\left(\pi \cdot K \cdot E^2 \cdot d\right) \\
\arcsin\left(\sqrt{T}\right) &= \pi \cdot d \cdot K \cdot \frac{V^2}{s^2} \\
\arcsin\left(\sqrt{T}\right) \frac{s^2}{\pi \cdot d} &= K \cdot V^2,
\end{aligned} \tag{3.2}$$

where T is the transmittance. The experimental data for the value of the left side of eq. (3.2) were plotted versus the square of the voltage V^2. The Kerr constant was derived from a linear fit to the slope. The obtained value is expected to be smaller than the true value of the bulk LC material because of neglecting the inhomogeneity of the in-plane switching electric field. However, the effective value of the Kerr constant obtained by this method is of practical importance. A peak finding algorithm was used to determine the operation voltage and to calculate the hysteresis according to eq. (2.12). To calculate the memory factor, 5 values were averaged at the beginning and the end of the measurement each before applying eq. (2.13).

3.3.3. Dynamic measurements

Dynamic measurements were performed to determine the switching times t_{on} and t_{off}, which are the response times of the liquid crystal composite, when the voltage is switched on and off, respectively. The temperature dependences of these response times were investigated.

At a certain temperature, the time dependent change of the intensity, when switching the voltage on and off, was recorded by the PMT detector (fig. 3.8).

A time period of 1 s was studied, while the voltage was applied or removed to measure t_{on} and t_{off}, respectively. The voltage applied to the test cell was equal to the operation voltage obtained from the Kerr experiment.

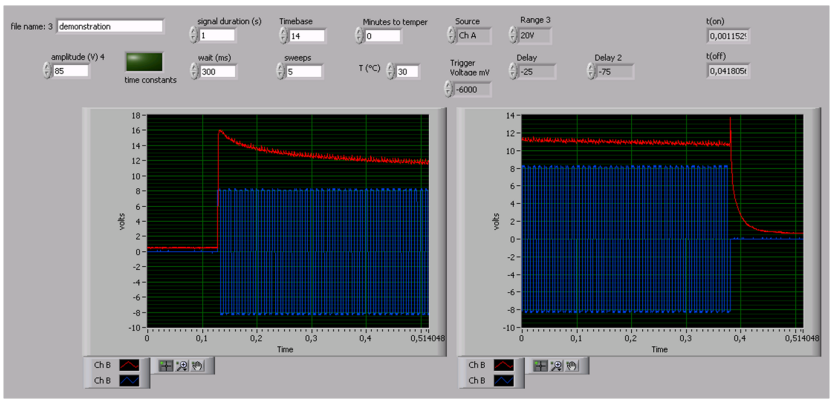

Figure 3.8.: View of the measurement routine used to measure the response times with the time dependent intensity changes and the applied square wave voltage for measuring t_{on} and t_{off} on the left and right side, respectively.

For all time-resolved data, the time differences were calculated for changes of the intensity from 0 % to 90 % and from 100 % to 10 % for t_{on} and t_{off}, respectively. In some cases, a very fast intensity change followed by a slow variation was observed. To distinguish these processes, an additional evaluation was applied. The fast part was calculated as the time difference between removal of the voltage and the onset of the slow process. The slow part was fitted by an exponential.

3.4. Photo-DSC

Photo-DSC was used to investigate the polymerization process. This method was applied after investigating a test cell containing the BP mixture of interest. In the following, equipment and experiment (section 3.4.1) and data analysis (section 3.4.2) are shortly presented.

3.4.1. Equipment and Experiment

A DSC 2 differential scanning calorimeter (Perkin Elmer) was modified to perform photo-DSC measurements and allow computer control of the device [49]. The photo-DSC instrument was equipped with a high pressure mercury lamp (Hönle

bluepoint 4) with two outgoing light guiding fibers. The photo-polymerization process was monitored synchronously.

The amount of sample was accurately weighted (about 10 mg) into a standard aluminium pan. An empty aluminimum pan was used as reference. A cover glass was placed above sample and reference to generate a nitrogen atmosphere in the chambers by a constant nitrogen purge (fig. 3.9). Temperature was adjusted to

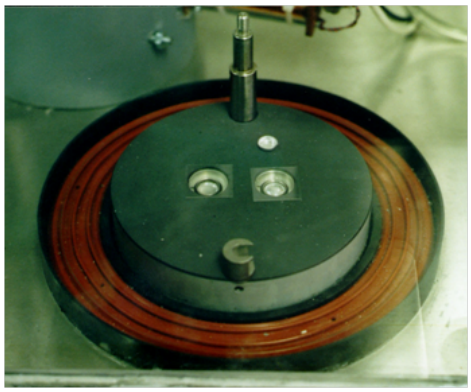

Figure 3.9.: Oven of the photo-DSC with sample (left) and reference (right) covered by a glass slide to keep the samples under nitrogen atmosphere.

the same value used before for photo-polymerization of the test cell. The measurements were carried out using polychromatic UV irradiation [72] with an intensity of $3\,\mathrm{mW\,cm^{-2}}$ and an exposure time of 6 min. One sample was illuminated twice: first, the time dependent heat flow is recorded and second the heat caused by light absorption is measured. It is crucial that the sample is totally polymerized under the existing conditions prior to the second illumination. The photo-DSC measurements were performed by Dr. Andreas Hoischen and Rita Egert-Tiesbohnenkamp.

3.4.2. Analysis of the photo-DSC data

The measurement of the heat flow caused by light absorption of the material was subtracted from the measurement of the total heat flow to obtain the conversion of the polymerization reaction. Based on the resulting heat flow $\frac{dH}{dt}$ of the polymerization, the rate of photo-polymerization R_p was calculated according to $R_p = \frac{dH}{dt}/\Delta H_{theor}$, where ΔH_{theor} is the maximum reaction heat when complete polymerization of the monomers in the system occurs. The functionality and the reaction enthalpies of the monomers were needed for this calculation. Because the exact reaction enthalpies of the substances used in this study were unknown, values

were taken from [74] being 86.11 kJ mol^{-1} and 54.76 kJ mol^{-1} per mole of acrylate and methacrylate groups, respectively. Through step-wise integration (the upper and lower sum of small time intervals were calculated) of the time dependent reaction rate (fig. 3.10a) the conversion (fig. 3.10b) of the photo-polymerization was obtained. All calculations were performed by Dr. Andreas Hoischen.

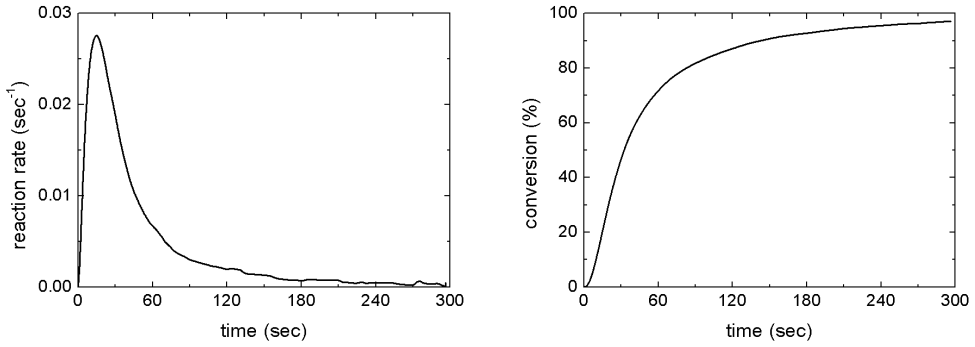

(a) **(b)**

Figure 3.10.: Time dependent reaction rate (a) and conversion (b) of a photo-polymerization reaction.

4. Results and Discussion

This chapter is divided into two parts: first results on BPs with visible Bragg reflections are presented and second systematically changed mixture compositions are analyzed with the intention to find the optimum composition for display application and to improve the polymerization process. In the first part (section 4.1), the phase sequence of the mixtures is elucidated and the switching process is analyzed in detail. Additionally, a method is presented, which indicates the degree of stabilization in samples with visible Bragg reflections. In the second part (section 4.2), the influence of chirality, monomer mass fraction, cross-linker fraction and cross-linker type on the electro-optic performance is discussed. Additionally, influences of polymerization temperature and UV exposure time are analyzed.

4.1. Differences between unpolymerized and polymerized samples

A model system, mixture 1 (table A.3) containing monomers, with Bragg reflections in the visible wavelength range was investigated to elucidate differences between unpolymerized and polymerized samples. As some measurement techniques require a white light source, additionally a pure BP mixture without monomers, mixture A (table A.1), was prepared to avoid unintentional polymerization during the investigation. The phase sequence (section 4.1.1) and the electro-optic performance (section 4.1.2) including the switching times (section 4.1.3) were investigated. Finally, a simple method to check the stability of PSBP with visible Bragg reflections is presented in section 4.1.4.

4.1.1. Phase sequences of BP and PSBP mixtures

The phase sequence of the samples was elucidated in a two-step process. First, POM was used to determine the temperature dependent phase transitions. Subsequently, Bragg reflection measurements were conducted in the BP range to confirm correct assignment of the different phases seen by POM. Here, the phase sequence

of the pure BP from mixture A and the PSBP from mixture 1 will be discussed in detail.

In fig. 4.1, the temperature dependent reflection wavelengths are shown for the pure BP observed in mixture A. In addition, POM pictures are added for specific temperatures. The pictures of the pure BP sample were taken while

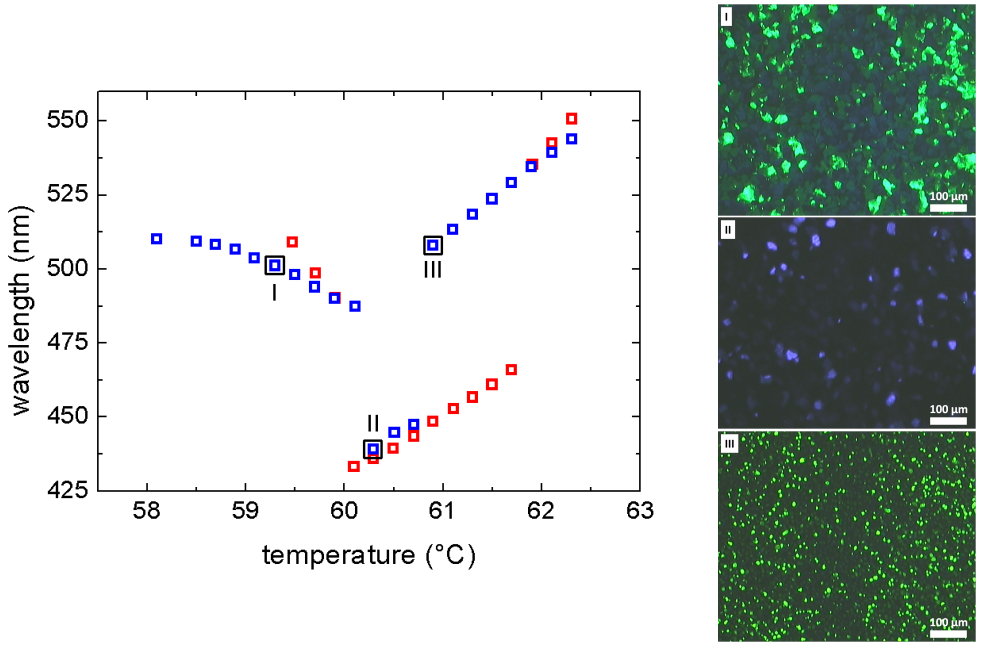

Figure 4.1.: The temperature dependent Bragg reflection maxima for the pure BP for heating (red squares) and cooling (blue squares) and some corresponding pictures taken by POM with (I) large green and dark blue platelets, (II) bright and dark blue platelets and black droplets and (III) small bright and dark green platelets with black droplets.

cooling, which explains the appearance of larger platelets at lower temperatures. The color changes (green–blue–green) of the platelets indicate two BP-BP transitions. This observation is confirmed by two discontinuous changes of the Bragg reflections (510 nm–435 nm–510 nm), which are known to indicate phase transitions (section 2.1.2). With increasing temperature, the first reflection is shifted to shorter wavelengths, while the reflections at higher temperature are both shifted to longer wavelengths. The transition temperatures differ for heating and cooling as well as the slope of the curves.

To further elucidate the phase sequence of the pure BP sample, the obtained Bragg reflections (fig. 4.1) were compared to literature [16, 19, 75]. In comparison with fig. 2.6, the blue-shift of the wavelengths reflected at low temperatures

indicates a BPI lattice. In rare occasions orange platelets have been observed in reflection, when cooling from the higher temperature BP to BPI. The reflection wavelengths of the orange platelets have not been measured, because this lattice orientation existed only for a very short time period before transforming in the lattice orientation with green reflection wavelengths. Therefore, the ratio of the two reflection wavelengths could not be determined and the lattice orientation remains unknown. Assigning the other two phases is not as trivial. The reflections of the higher temperature BPs (fig. 4.1I and fig. 4.1II) do not coincide with any reflections in fig. 2.6. The reflection of BPII is expected to be temperature independent, but instead the reflection we observe after the phase transition shifts to longer wavelengths with increasing temperature. For clarification, the Bragg measurement was repeated with a different cell, which induces planar alignment, filled with mixture A. The slightly different phase sequence is depicted in fig. 4.2. This time, a constant reflection with short reflection wavelength appears in a

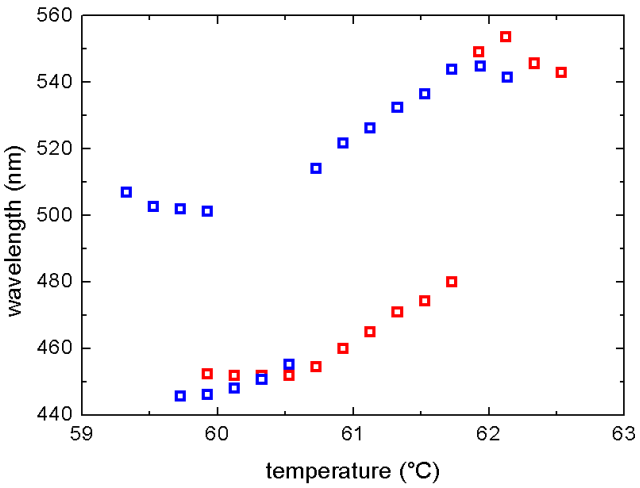

Figure 4.2.: Bragg reflections of mixture A in a cell with planar alignment measured for heating (red) and cooling (blue).

range from 59.9 °C to 60.5 °C. At temperatures larger than 60.7 °C, the reflection smoothly shifts to longer wavelengths. By comparison to the sequence measured while cooling, it can be confirmed that this reflection is the one following BPI in the phase sequence. The range of constant selective reflections is assigned to be BPII in agreement with ref. [16]. Still the continuous change to a red-shifted reflection needs to be explained.

Flack and Crooker [19] had observed first order and second order transitions from BPI to BPII, which lead them to the conclusion that two different BPII modifications exist. This behavior was only observed in LC mixtures and never in a pure compound. Therefore, more detailed investigations have been performed by Marcus [75], who disproved the existence of two BPII modifications. Marcus identified the continuous transition as transition to a coexistence region of BPI and Iso. He confirmed that the first order transition really was a BPI to BPII transition.

In our study, also LC mixtures containing several compounds were used as nematic host. Consequently, a schematic phase diagram (fig. 2.2), in which phases are separated by coexisting regions, was used to fully explain the phase sequence observed in our pure BP sample. The phase sequence of mixture A follows the

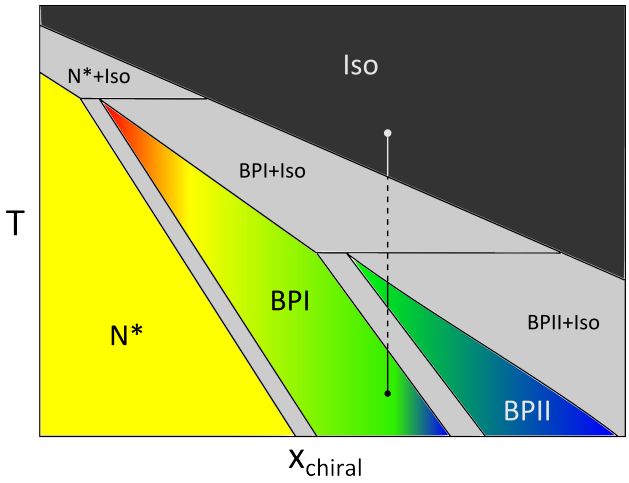

Figure 4.3.: Schematic phase diagram with transition regions instead of explicit transition temperatures. The vertical line follows the phase sequence observed by POM in mixture A with increasing temperature.

vertical line within the phase diagram. As mentioned above, first a N^* to BPI transition is observed. Subsequently, a coexisting region of BPI and BPII may (fig. 4.2) or may not (fig. 4.1) be observed, depending on heating and cooling rates during the measurement. The appearance of BPII also depends on the speed of the temperature changes. A large coexistence region of BPII and Iso as well as a coexistence region of BPI and Iso at even higher temperatures are visible. This reentrant behavior (phase sequence BPI–BPII-BPII/Iso–BPI/Iso) can be explained as follows: In mixtures, where the clearing temperature decreases with

increasing fraction of the chiral component, the BP/Iso two-phase region is characterized by spontaneous phase separation into a more chiral isotropic phase and a less chiral blue phase. To preserve the equilibrium state of the system, the total amount of the more chiral isotropic phase increases with increasing temperature at the expense of the chiral fraction of the remaining BP islands. Thus, an initially stable BPII may transform to BPI on increasing temperature as soon as the chiral concentration in the BP islands drops below a critical value. This explanation is also supported by POM. At temperatures where coexistence of BPII and Iso was suggested based on Bragg reflection measurements black regions emerge next to the BP platelets indicating the isotropic phase. The Iso parts grow with increasing temperature, while the BP areas become smaller including a color change of the platelets.

Having analyzed the phase sequence of the pure BP sample, the temperature dependent phase behavior of the PSBP is elucidated next. In fig. 4.4, the temperature dependent Bragg reflection wavelengths are depicted together with corresponding POM pictures showing the textures at specific temperatures. The PSBP

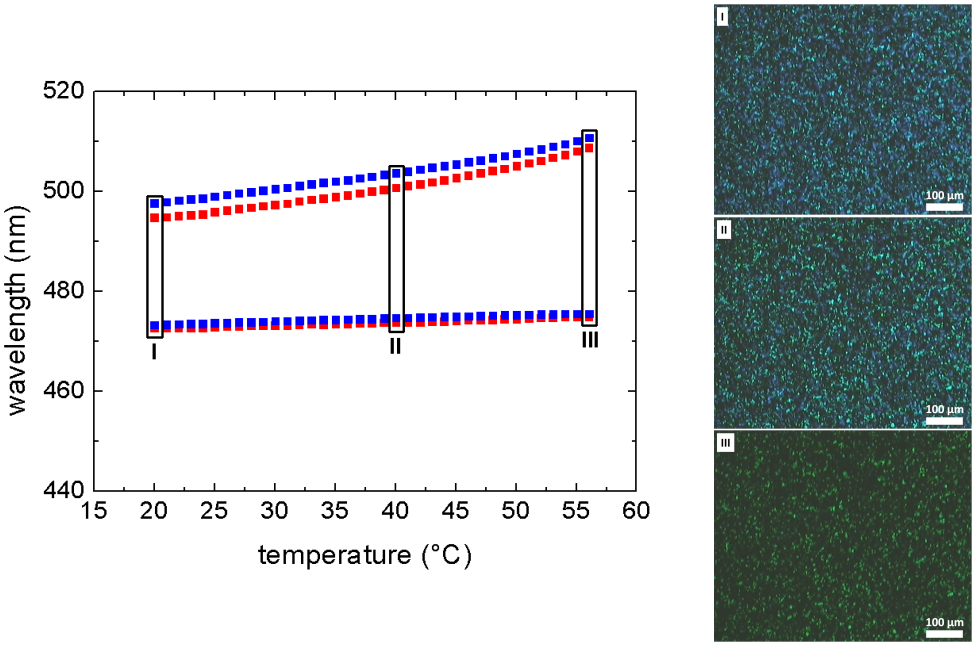

Figure 4.4.: The temperature dependent Bragg reflection maxima for the PSBP for heating (red squares) and cooling (blue squares) and some corresponding pictures taken by POM with (I) many blue and a few green platelets, (II) blue platelets, green platelets and black droplets and (III) green platelets with black droplets.

shows two reflection maxima, one at 475 nm and one at 495 nm representing the blue and green platelets in picture 4.4I, respectively. The green reflection shows a clear red-shift with increasing temperature, while the blue reflection is hardly affected by the temperature change. As seen in the pictures 4.4I–4.4III, the amount of green platelets increases with temperature, while the amount of blue platelets decreases. This results in intensity changes within the spectra (fig. 4.5). In the range from 20 °C to 56 °C, the intensity of the blue reflection decreases with temperature, while the intensity of the green reflection increases with temperature.

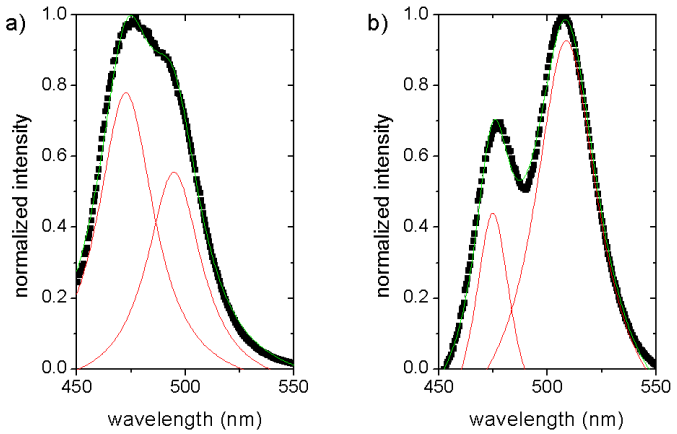

Figure 4.5.: Normalized intensities of the Bragg peaks (a) at 20 °C showing a large peak at 475 nm with a shoulder at 495 nm, and (b) at 56 °C showing two separated peaks at 475 nm and 510 nm. The fitted peaks (red) sum up to the total intensity of the selective reflections (green).

Once the phase sequence of the pure BP without polymer network is determined, analyzing the reflections of the PSBP is less complicated making use of the already obtained insights. The green and blue reflections observed in fig. 4.4 correspond to BPI and BPII, respectively. This indicates that a coexistence region of these two phases was stabilized by in-situ photo-polymerization. The absence of discontinuities in the Bragg reflection measurement proves that no first order transitions occur in the sample. Seemingly second order transitions were associated with continuous changes of Bragg reflections like the red-shifts observed in coexistence regions of BP and Iso due to depletion of the chiral component in the BP. Therefore, the changes observed by POM are used for further interpretation. The texture in picture 4.4I shows the coexistence of BPI and BPII, green and blue

platelets respectively. The additional appearance of dark spots in picture 4.4II indicates coexistence of BPI, BPII and Iso. In picture 4.4III only BPI coexists with Iso, while the Bragg measurement still shows both Bragg peaks even so the intensity for the blue reflection decreases (fig. 4.5). This difference is caused by the fact that pictures could not be taken at the same time as the Bragg measurement was performed and temperatures were adjusted manually. As shown for the pure BP, the sample composition in a coexistence region changes with temperature so that the sample prevails in the equilibrium state. Here, we observe coexistence of three phases, which makes the prediction of the changes more difficult. The disappearance of BPII in picture 4.4 might result from a change of BPII to the isotropic phase, which would explain the absence of a discontinuous change of the reflection wavelength. On the other hand, a very slow transformation of BPII to BPI, which is smeared by the equilibrium formation, seems possible. Based on the present data, the disappearance of BPII can not be fully explained. But it seems that BPI is better stabilized by the formed polymer network than BPII.

In conclusion, the pure BP mixture A has the phase sequence N^*–BPI–BPII–BPII/Iso–BPI/Iso–Iso, when the temperature is slowly increased. In contrast, PSBP remains in the stabilized BP unless the transition to the isotropic phase occurs. If coexistence regions were stabilized, the sample probably adjusts to the equilibrium condition at each temperature. This may result in shifts of the reflection wavelength as observed for the pure BP.

In the next section, electro-optic properties of unpolymerized and polymerized BPs will be analyzed.

4.1.2. Anomalies affecting the Kerr measurement

To illustrate the benefits offered by polymer-stabilization, test cells were investigated before and after photo-polymerization according to the procedure described in section 3.3.2. Normalized voltage-transmittance curves for three temperatures are shown for the unstabilized (figs. 4.6a and 4.6c) and stabilized samples (figs. 4.6b and 4.6d) containing mixture 2 (table A.4) or mixture 1 (table A.3), respectively. These mixtures contain different kinds of cross-linker non-mesogenic HDDMA and mesogenic BPRM-2 as well as different fractions of the chiral dopant 3.8 wt% and 2.8 wt% for mixture 2 and mixture 1, respectively. The corresponding phase transition and polymerization temperatures are shown in table B.11. In the unpolymerized samples, the curves correspond to temperatures of the N^* to BP transition (blue), BP (green) and Iso (red). In the polymerized samples, two curves corre-

spond to BP temperatures (blue and green) and fig. 4.6b additionnally includes a curve measured in the isotropic phase (red). Despite different cross-linkers and chirality, the general behavior is the same for mixture 1 and mixture 2. Hence, only mixture 2 will be discussed in detail.

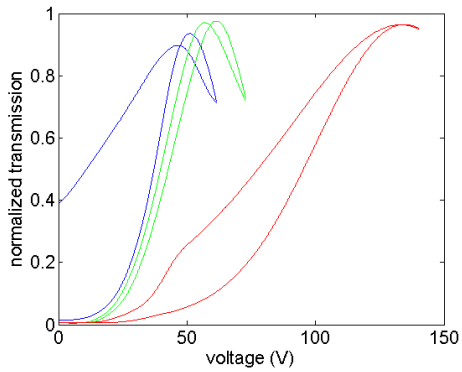

(a) Unpolymerized mixture 2 at 27.8 °C, 31.8 °C and 35.8 °C

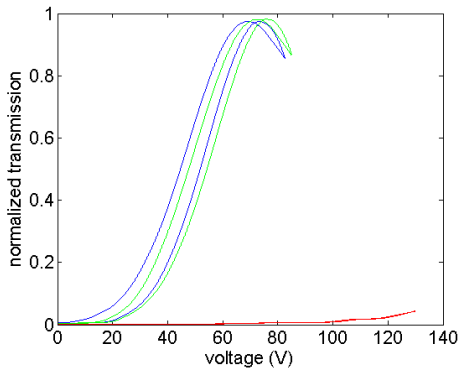

(b) Polymerized mixture 2 at 20 °C, 40 °C and 60 °C

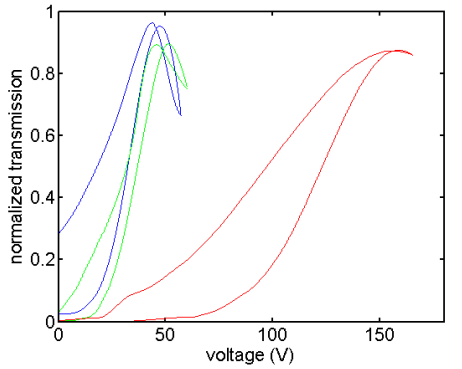

(c) Unpolymerized mixture 1 at 41.7 °C, 44.7 °C and 47.7 °C

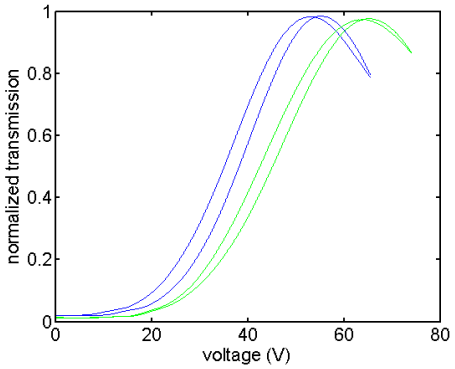

(d) Polymerized mixture 1 at 20 °C and 40 °C

Figure 4.6.: Voltage dependent transmittance curves with increasing temperature from blue to red for mixture 2 (a–b) and mixture 1 (c–d) in the unpolymerized and polymerized state. The temperatures chosen correspond to N^* to BP transition (blue), BP (green) and Iso (red) in the unpolymerized samples and to BP (blue, green) and Iso (red) in the polymerized samples. The anomalies appearing near the phase transitions of the unpolymerized samples do not occur in the stabilized samples.

A temperature range of 8 K was investigated for the unpolymerized sample (fig. 4.6a). At the N^* to BP transition temperature hysteresis is large and a transmittance of 40 % remains at the end of the measurement. In the BP at higher temperature the operation voltage is slightly increased, hysteresis is small and no residual birefringence occurs. Hysteresis is increased again in the isotropic phase and an additional kink appears when voltage is reduced. Additionally, operation voltage is about 2.5 times higher than in the BP.

POM observations of the unstabilized mixture 1 have shown that an electric field easily induces the chiral nematic phase near the the N^* to BP transition temperature. When the voltage is removed the BP platelets form very slowly. As the measurement is faster than the platelet formation, light scattered by chiral nematic areas of the sample contributes to the remaining transmittance at the end of the measurement.

Large hysteresis is another effect resulting from the completely different time scales of the field-induced phase transition and the platelet formation appearing for increasing and decreasing voltage, respectively. In BP, the sample behaves as expected showing acceptable hysteresis and no residual birefringence. The kink observed in the isotropic phase may result from a phase transition. Higher ordered phases can be electrically induced. Such an induced phase would relax back to the isotropic state, if the applied voltage becomes too low. It is also plausible that a higher ordered phase exhibits larger birefringence and thus larger transmittance than the isotropic phase, which results in larger hysteresis. In general, the operation voltage increases continuously with temperature. At the BP to Iso transition also discontinuities are possible and the slope becomes more steep (see section 4.1.3 fig. 4.7). Accordingly, a 2.5 times higher operation voltage in the isotropic phase than in the blue phase is not surprising.

On the other hand, the polymer-stabilized sample (fig. 4.6b) with a BP temperature range of nearly 40 K, does neither show residual birefringence nor any kinks. The two curves measured in the BP look very similar. The only difference is the higher operation voltage required to measure the curve at higher temperature. In contrast, the red curve measured in the isotropic phase shows hardly any transmittance for the applied voltages up to 130 V.

The polymer network stabilizes the disclination network of the BP. Consequently, the BP temperature range is significantly increased, about 35 K in mixture 2. At the same time, both operation voltage and hysteresis increase compared to the unpolymerized sample. The increase of the operation voltage probably re-

sults from anchoring forces between polymer network and LC. Deformation of the polymer network in the electric field, which even might not relax back to the undeformed state, contributes to the larger hysteresis. The latter effect is stronger in weaker polymer networks. BP with a rigid polymer network benefit from suppression of undesired effects such as residual transmittance and electrically induced phase transitions, which deteriorate the electro-optic response of unstabilized samples, especially near phase transition temperatures.

While in this section the main focus was on the influence of polymer-stabilization on the static parameters of the sample, its influence on the dynamic processes is investigated in the next section.

4.1.3. Switching processes with different speed

The response times t_{on} and t_{off} are of general interest for display applications. In this section, the response times of the unpolymerized and polymerized state of mixture 1 are discussed in detail. It is interesting to see, whether the dynamic response of the Kerr effect for the unstabilized and stabilized BP differs since the static properties of the Kerr effect are different.

The response times were measured and analyzed as described in section 3.3.3. In fig. 4.7, t_{on} and t_{off} and the operation voltage at different temperatures are shown for the unpolymerized sample (fig. 4.7a) and the polymerized sample (fig. 4.7b). The unpolymerized sample (fig. 4.7a) was investigated in a temperature range from 41.6 °C to 45.8 °C. It shows a temperature independent response time t_{on} of about 1 ms and a highly temperature dependent response time t_{off} with values between 140 ms and 1 ms for low and high temperatures, respectively. With increasing temperature, the operation voltage increases from 40 V to 60 V in the BP and shows a steep increase from 80 V to 130 V in the isotropic phase. For the polymerized sample (fig. 4.7b), a much larger temperature range from 20 °C to 55 °C was investigated according to the thermal stabilization. Response times decrease with increasing temperature from 1.8 ms to 0.75 ms and 9 ms to 1 ms for t_{on} and t_{off}, respectively. At the same time, the values in the PSBP are constant for temperatures above the N^* to BP transition of the unstabilized sample. The voltage increases continuously from 50 V to 70 V with increasing temperature.

Comparing the unpolymerized with the polymerized sample, some differences are obvious. The BP range is about 30 K wider in the polymerized state than in the unpolymerized state and the PSBP required a 10 V higher operation voltage. Also the response times show significant differences. While t_{on} is constant for

both samples above 41.6 °C, it increases for lower temperatures in the polymerized sample. This effect might be attributed to higher viscosity of the LC at low temperatures, which probably results in slower reorientation of the molecules. While the same observation applies to t_{off} of the polymerized sample, it is more difficult to explain the significantly slower response t_{off} of the unpolymerized sample. This response is about 10 times slower in the BP and becomes fast only in the isotropic phase.

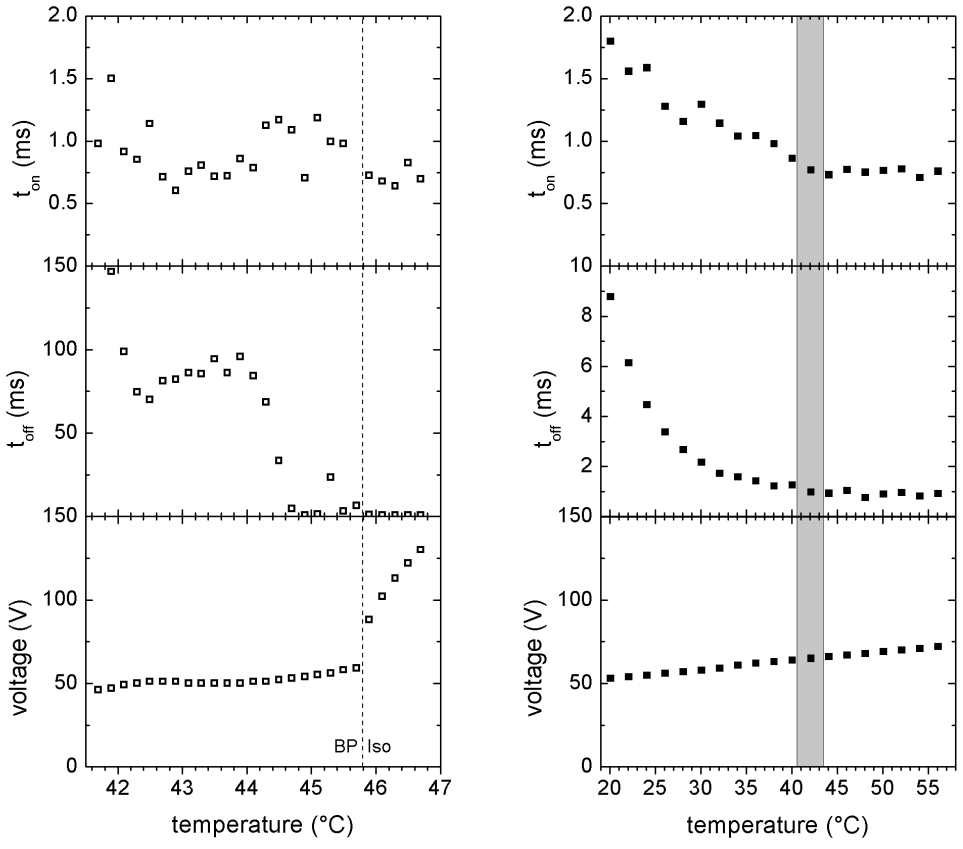

Figure 4.7.: Response times and operating voltages for the unpolymerized sample (a) and the polymerized sample (b). The dashed line indicates the BP to Iso transition temperature of the unpolymerized sample. The measured temperature range of the unpolymerized sample (a) is indicated by a gray background in (b) to highlight the quite different temperature ranges of BP stability.

To determine the origin of the slow contribution to the response time t_{off} in the unstabilized sample, a more detailed look on the original data was necessary. The intensity versus time curves for three temperatures are depicted in fig. 4.8. The analyzed temperatures correspond to the N^* to BP transition and one temperature in the BP and the isotropic phase each. The data were analyzed as described in section 3.3.3 for the additional evaluation of the fast and slow processes. The applied voltages are about 1 V higher than V_{op} of the sample. Therefore, spikes may appear when the voltage is switched of as in fig. 4.8b.

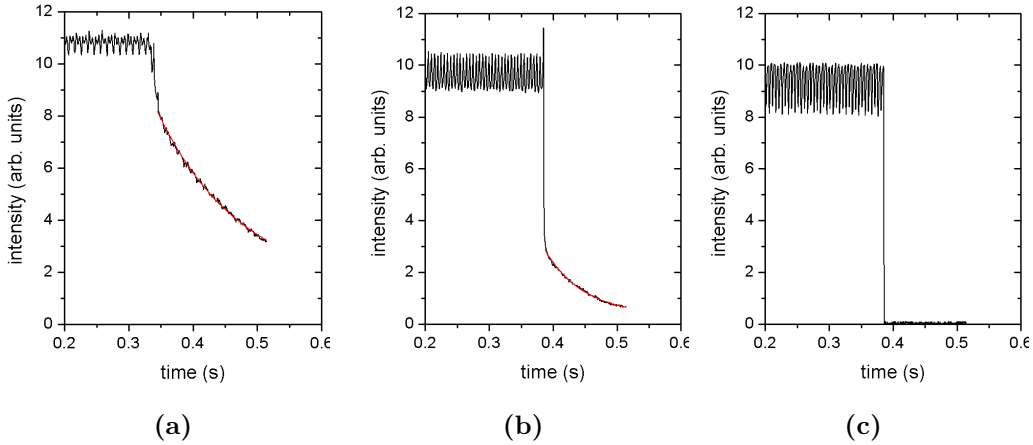

Figure 4.8.: Response of the unpolymerized sample when switching the voltage off for (a) the N^* to BP transition at 41.9 °C, (b) BP at 44.3 °C and (c) Iso at 46.1 °C. The red line corresponds to the exponential fit used to evaluate the slow response.

At the N^* to BP transition (fig. 4.8a) the response is composed of a small part which is fast and a larger part which is slow. At the end of the measurement residual transmittance of more than 25 % remains. As already mentioned in section 4.1.2, the residual transmittance results from light scattered by chiral nematic areas of the sample, which have not yet transformed to BP platelets again in the short time period of the measurement. As observed by POM, platelet formation may take several minutes. In the BP (fig. 4.8b) also a fast and a slow part contribute to the response. However, the contribution of the slow part is smaller. At this temperature, the process of platelet formation could not be observed by POM, probably because it was too fast. Consequently, the slow process occurring in the BP of the unstabilized sample might have a different origin such as electrostriction

[18]. The remaining intensity at the end of the measurement is less than 10 %. In the isotropic phase (fig. 4.8c) only the fast process contributes to the response time and no residual intensity remains.

In conclusion, field-induced phase transitions may lead to extremely slow responses especially near the N^* to BP transition temperature. However, it is not clear whether the slow contribution to the response time t_{off} only results from field-induced phase transitions. If there is an other slow process, it still needs to be identified.

For further investigations, the voltage dependent Bragg reflections were measured. The voltage dependent changes of the reflected wavelengths are shown in fig. 4.9 for the pure BP mixture A. At the beginning of the measurement the

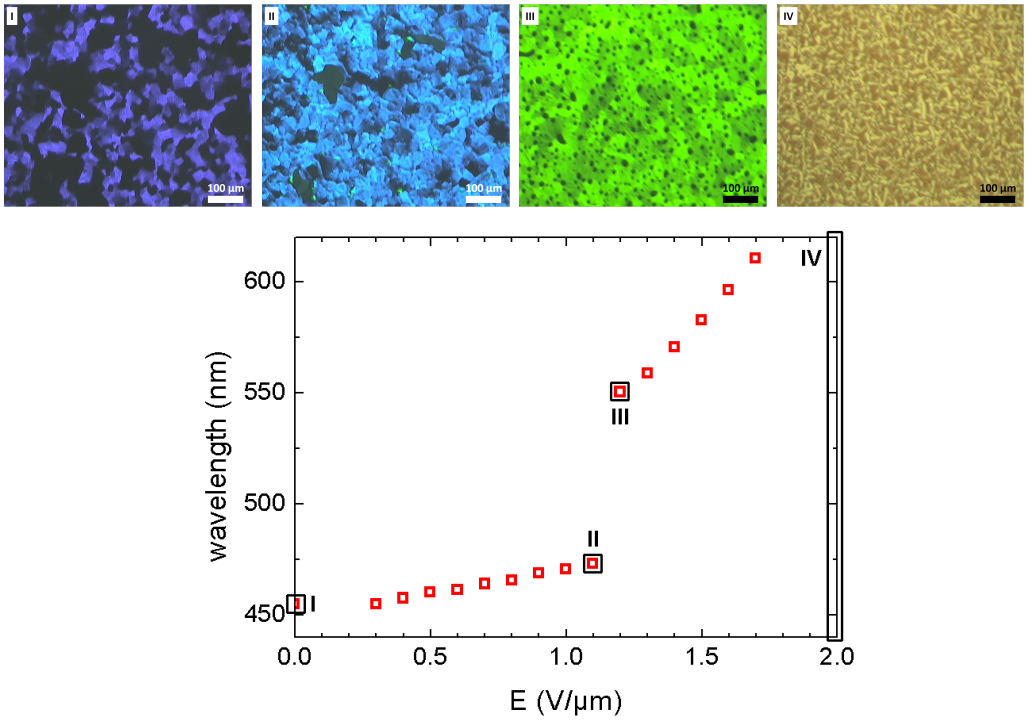

Figure 4.9.: Voltage dependent Bragg reflections of a pure BPII sample for increasing voltage and corresponding POM pictures with (I) bright blue platelets and some darker platelets, (II) light blue platelets, some darker spots and emerging green platelets, (III) a light green area with some darker spots and (IV) focal conic texture of the chiral nematic phase.

sample exhibited BPII (fig. 4.9I), which was identified by the blue platelets according to section 4.1.1. With increasing electric field, the reflection maximum is continuously shifted to longer wavelengths and a discontinuous change appears

at about 1.2 V/µm. The continuous change of the selective reflection results from electrostriction of the BP lattice, while the discontinuous change indicates a BP–BP transition as discussed in section 4.1.1. In fig. 4.9II, the emerging small green platelets are the first signs of the transition, which is complete in fig. 4.9III where the green reflection prevails. In fig. 4.9IV, which was taken at 2 V/µm, the BP has completely transformed to the chiral nematic phase, which strongly scatters light. Assuming that the unstabilized mixture 1 reacts similar to the electric field as sample A, for which the Bragg reflections were measured, the slow contribution to the response time t_{off} in fig. 4.8b can be identified as a combination of electrostriction and field-induced BP–BP as well as BP–N* transitions.

The field-dependent change of the Bragg reflections was measured for the polymerized mixture 1 as well. The results are shown in fig. 4.10. In PSBP, the reflection wavelengths only change slightly, when the applied field becomes larger than 0.3 V/µm. For higher electric fields, the wavelength of the selective reflection is constant. The change is hardly visible by POM. The platelets are brighter in picture 4.10I and darker in picture 4.10II, where the amount of isotropic areas is increased, but in both cases the reflection is of blue-violet color. As the change only appeared when the electric field was applied for the first time, it is probably a hysteresis effect, which can be neglected for repeated switching of the sample. The absence of continuous and discontinuous changes indicates that the BP is more stable after polymerization. Consequently, electrostriction and field-induced phase transitions are suppressed, which explains the faster response time t_{off} in the polymerized sample fig. 4.7b.

This section can be summarized as follows: Starting with a comparison of the dynamic response of the Kerr effect for mixture 1 in the unpolymerized and polymerized state (fig. 4.7), the most remarkable difference appeared for the response time t_{off}. In the following, the exceptionally slow response time of the unstabilized sample was investigated in detail based on the original data from the dynamic measurements and additional Bragg reflection measurements. A fast and a slow contribution to the response time t_{off} were found. They are separately depicted in a histogram in fig. 4.11 as blue and orange bars, respectively. These bars add up to the response time. In fact, the slow contribution only affected the unstabilized sample and it is up to 10 times slower than the fast process. The response near the N* to BP transition is extremely slow because of the particularly slow platelet formation after the chiral nematic phase was induced by the electric field. The slow contribution results from a combination of lattice distortions and field-in-

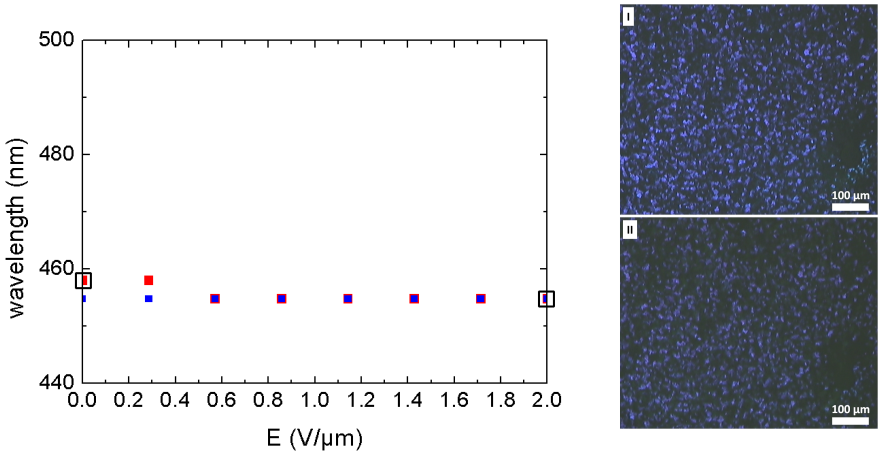

Figure 4.10.: Voltage dependent Bragg reflection maxima for the PSBP for increasing (red squares) and decreasing (blue squares) voltage and some corresponding pictures taken by POM with (I) blue platelets and some dark spots and (II) blue platelets and more dark areas.

duced phase transitions. In contrast, the fast process results from local molecular reorientations in the electric field. All these effects contribute to the Kerr effect. As a fast response of the sample is desired for display applications, it is welcome that the slow processes are suppressed in polymer-stabilized blue phases.

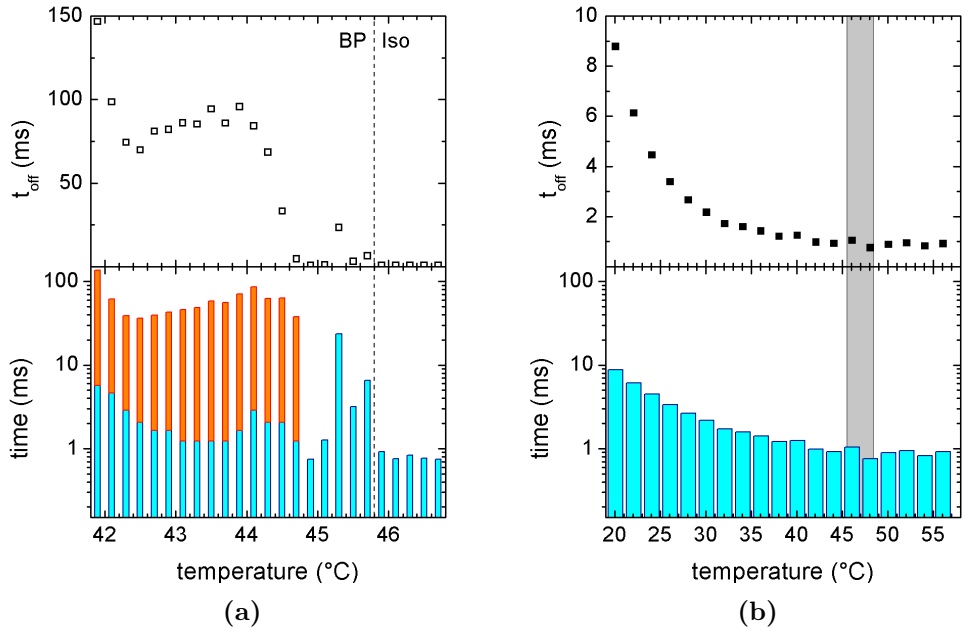

Figure 4.11.: The same data for t_{off} as in fig. 4.7 for the unpolymerized sample (a) and the polymerized sample (b). The contributions of the fast switching process (blue) and of the slow switching process (orange) are represented in the histograms with logarithmic scale. In the stabilized sample only fast switching occurs.

4.1.4. Stability of polymer-stabilized blue phase

In sections 4.1.1 to 4.1.3, the positive impact of the polymer network on the electro-optic performance of PSBP was demonstrated, including a broader BP temperature range and faster response time. Here, we present a simple way to check on the stability of the formed polymer network in PSBPs with visible Bragg reflections.

After polymerization, the PSBP shows a certain platelet texture at room temperature (RT). If the polymer network stabilizes this BP structure, the same platelets are expected to show up again, when the sample is cooled to RT from the isotropic phase. To test this, pictures of the texture need to be taken at the beginning and the end of the experiment. By comparing the textures in these pictures, it is possible to judge whether the stability of the polymer network is sufficient or not.

In my experiment, the same platelet texture that was initially observed at RT (fig. 4.12a) reappeared at RT after thermally inducing the isotropic phase

fig. 4.12b. As the platelets of this sample are relatively small, one area was enlarged for better comparison. During the thermal treatment a little flow was induced in the texture, which brought it out of focus. Therefore, the exact shape of the platelets in not apparent in the inset in fig. 4.12b. Nevertheless, the same platelets as in fig. 4.12a can be identified and their shape is similar. This indicates a good stabilization of the BP by the polymer network.

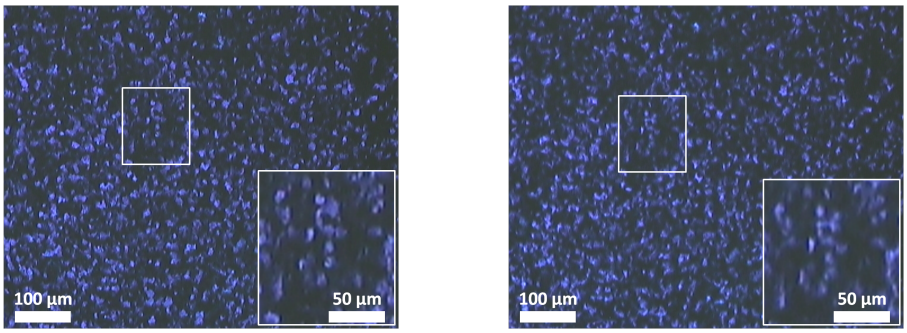

(a) **(b)**

Figure 4.12.: Platelet texture at RT before (a) and after (b) the isotropic phase was thermally induced. For better comparison, insets show an enlarged platelet configuration.

This experiment not only works for thermal treatment of the sample, but also when the chiral nematic phase is induced electrically and the voltage is removed subsequently. The textures taken at 0 V before (fig. 4.13a) and after (fig. 4.13b) inducing N^* are identical. This indicates that the electric field does not deform the polymer network in a lasting manner.

In brief, a fast and easy method to investigate the stability of the polymer network to changes of the thermal environment or electrical fields was presented. Of course, this experiment works only for samples with visible Bragg reflections and not for samples with Bragg reflections in the UV range, for which composition effects are investigated in the following sections.

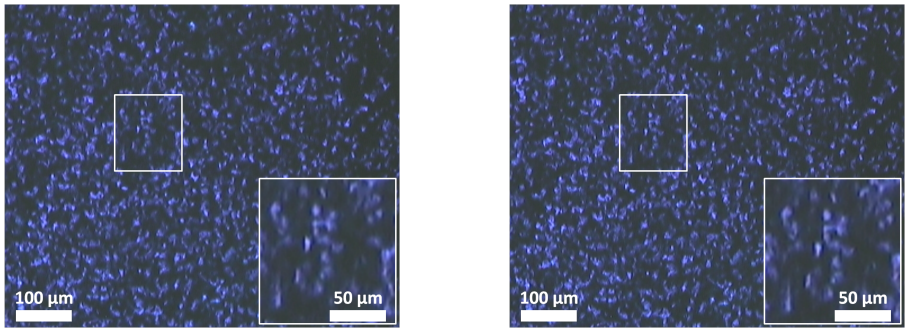

(a) (b)

Figure 4.13.: Platelet texture at RT and 0 V before (a) and after (b) the chiral nematic phase was electrically induced. For better comparison, insets show an enlarged platelet configuration.

4.2. Influence of different parameters on the electro-optic performance

For a specific BP system, the electro-optic performance of the sample is influenced by sample composition and preparation conditions. The composition was changed systematically to investigate influences of chirality (section 4.2.1), monomer mass fraction (section 4.2.2), and cross-linker fraction (section 4.2.3) using HDDA as cross-linker. Some of the experiments were repeated with different kinds of cross-linkers. The respective results are presented in section 4.2.4. The standard procedure for cell preparation described in section 3.2 was developed at Merck Darmstadt. Additional investigations on polymerization temperature (section 4.2.5) and UV exposure time (section 4.2.6) were performed with our setup.

4.2.1. Chirality

The BP model systems used in section 4.1 contained 2.8 wt% chiral dopant, while in the following sections 4.2.2 to 4.2.6, BP systems containing 3.8 wt% chiral dopant were investigated. Because of the different chirality, the Bragg reflection wavelengths of these mixtures differ. In this section, it is investigated whether this change of chirality also affects the electro-optic performance (operation voltage and hysteresis) of the sample. Therefore, five mixtures (table A.5) with a monomer fraction $\chi_w = 10$ wt%, composed of 6 wt% BPRM-1 and 4 wt% HDDA, and varying chirality between 2.8 wt% and 3.8 wt% were investigated. The selective reflections of the mixture containing 2.8 wt% chiral dopant were clearly in

the visible wavelength range, while those of the mixture containing 3.0 wt% chiral dopant were barely visible. The three other mixtures had selective reflections only in the UV wavelength range. The respective phase sequences and polymerization temperatures are listed in table B.12.

The chirality-dependent operation voltage (black) and hysteresis (red) of PSBP are plotted in fig. 4.14. In this representation, the bars indicate the range between

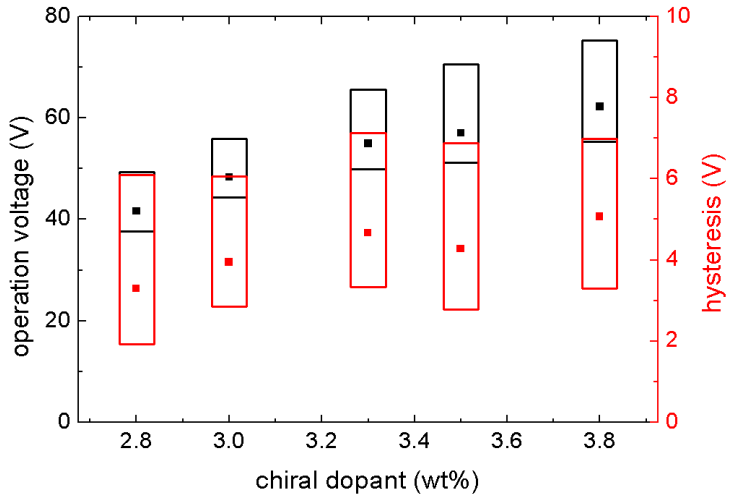

Figure 4.14.: Chirality-dependent operation voltage (black) and hysteresis (red) for PSBP containing 6 wt% BPRM-1 and 4 wt% HDDA. The bars indicate the range between the lowest and the highest value within a temperature range from 20 °C to 54 °C. Additionally, the mean value (square) is shown.

the lowest and the highest value measured in a temperature range from 20 °C to 54 °C. The mean value is marked by a square, which is not necessarily located at half height of the bar. The same representation is used in the following sections.

Figure 4.14 shows that the operation voltage increases with increasing fraction of the chiral dopant. The hysteresis is quite constant for the investigated chiralities, although the smallest hysteresis value and the lowest mean value were observed for the mixture with 2.8 wt%.

The correlation of operation voltage and chirality in pure BP mixtures without monomers was already studied in my master thesis [76]. The results are shown in fig. 4.15, which is extended to some additional chiralities. In ref. [70], the corresponding temperature dependent Kerr constants are shown. For these mixtures, composition and phase sequence are listed in table A.9 and table B.16, respectively. Most interesting is the observation that the operation voltages in the

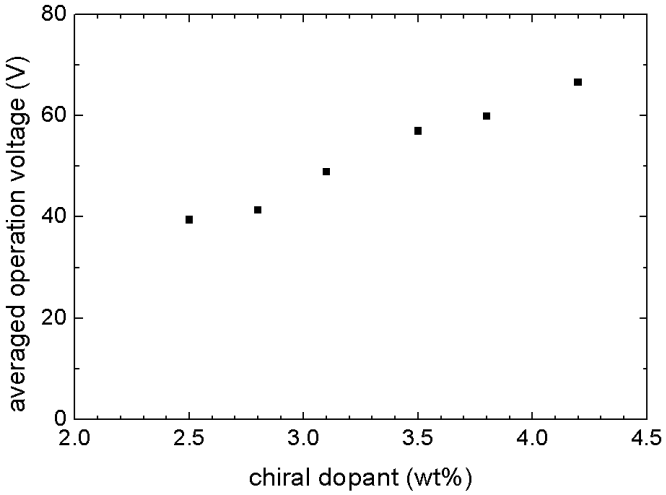

Figure 4.15.: Chirality dependent operation voltage (black) and hysteresis (red) for BP mixtures without monomers. The operation voltage was averaged for the BP range of each mixture, which changed with the fraction of chiral dopant. With increasing amount of the chiral dopant, the BP range in the mixtures became broader and the clearing temperature was shifted to lower temperature.

polymerized mixtures (fig. 4.14) and the mixtures without monomers (fig. 4.15) are very similar, regardless of the presence or absence of a polymer network. It can be concluded from this observation that the operation voltage depends mainly on the intrinsic properties of the nematic LC, which is well separated from the polymer network in the PSBP mixtures. The almost constant hysteresis observed for the PSBP mixtures indicates a similar degree of stabilization for all chiralities when polymerizing 6 wt% BPRM-1 and 4 wt% HDDA. With about 8 % of the operation voltage, the hysteresis in the IPS cells was relatively large, but in the same range as reported in refs. [20, 22, 77] for commonly used BP systems.

For fundamental investigations on the properties of PSBP (section 4.1) low chiralities are preferred, while higher chiralities are needed for display applications (section 4.2). Mixtures containing a monomer fraction of $\chi_w = 10$ wt% and a ratio of mono- and di-functional monomer of 3:2 allow polymer-stabilization of mixtures with low and high chirality. They also provided stabilization when single substances were exchanged, for example the cross-linker (section 4.2.4). Because of this general ability to stabilize BP under various conditions, mixtures with this composition of mono- and di-functional monomers can be used as standard mixtures.

With regard to display applications, the chiral dopant fraction needs to be high enough to shift the Bragg reflections into the UV wavelength range. At the same time, it should be as low as possible to reduce the operation voltage of the device, which increases with increasing amount of chiral dopant. According to the presented data, the mixture containing 3.3 wt% of the chiral dopant complied best with these conditions.

4.2.2. Total monomer content

The polymer network located in the disclination lines stabilizes the BP structure as discussed in section 2.5.1. For adequate stabilization, it is expected that these defect regions are completely filled with polymer network. At the same time, complete polymerization of the monomers is required to achieve segregation of polymer and LC. Therefore, it is important to optimize the monomer fraction in the mixture.

In this study, mixtures containing BPRM-1 and HDDA in a ratio of 3:2 were investigated for monomer mass fractions from 8 wt% to 12 wt%. For the exact composition of the mixtures, see table A.6. Additionally, phase transitions and polymerization temperature are listed in table B.13. In fig. 4.16, the operation voltage (black) and the hysteresis (red) of these mixtures are depicted depending on the fraction of monomers. The operation voltage has a tendency to increase with increasing monomer fraction from 8.1 wt% to 9.4 wt% and from 11 wt% to 12 wt%. However, no significant differences of the operation voltage were observed for the mixtures with monomer fractions between 9.4 wt% and 11 wt%. The hysteresis is similar for all mixtures in absolute values, but relatively to the operation voltage it decreases from 7 % to 6 % with increasing monomer fraction.

Typically, monomer fractions between 8 wt% and 15 wt% are required to stabilize a conventional BP mixture [12, 63]. In the mixtures presented above, successful stabilization was achieved for all monomer fractions from 8 wt% to 12 wt%. Because of the reverse trends for operation voltage and hysteresis, a trade-off is necessary when choosing the monomer fraction of a BP mixture.

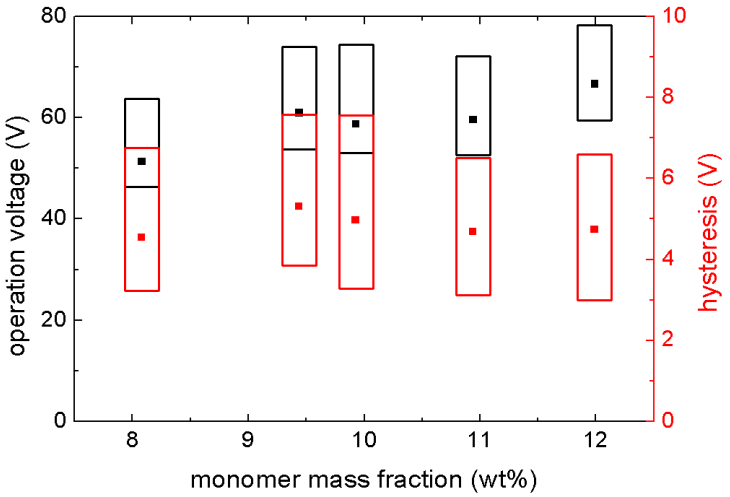

Figure 4.16.: Monomer fraction dependent operation voltage (black) and hysteresis (red) for mixtures containing BPRM-1 and HDDA at a ratio of 3:2. The bars indicate the range between the lowest and the highest value within a temperature range from 20 °C to 54 °C. Additionally, the mean value (square) is shown.

4.2.3. Cross-linker fraction

The degree of cross-linking affects the stability and the stiffness of the polymer network. Mixtures containing 12 wt% monomer were investigated and the fraction of the cross-linker HDDA was changed between 3.2 wt% and 7.2 wt%. The exact compositions of the mixtures are given in table A.7a and phase transition and polymerization temperature are listed in table B.14.

The operation voltage (black) and the hysteresis (red) for these mixtures are shown in fig. 4.17 for a temperature range from 20 °C to 50 °C. Operation voltage and hysteresis are slightly lower for HDDA fractions above 5 wt%. Additionally, the minimum and maximum value of the hysteresis are closer together when the fraction of HDDA is larger than 5 wt%.

In addition to the electro-optic characterization, photo-DSC measurements were performed. The reaction rate of the polymerization (a) and the conversion (b) are shown in fig. 4.18. High conversion is observed for mixtures containing up to 5 wt% HDDA. Both mixtures with higher fractions of the cross-linker show reduced conversion. For the mixtures with reduced conversion, a larger amount of residual monomers remains in the mixture. This may result in a lower clearing temperature.

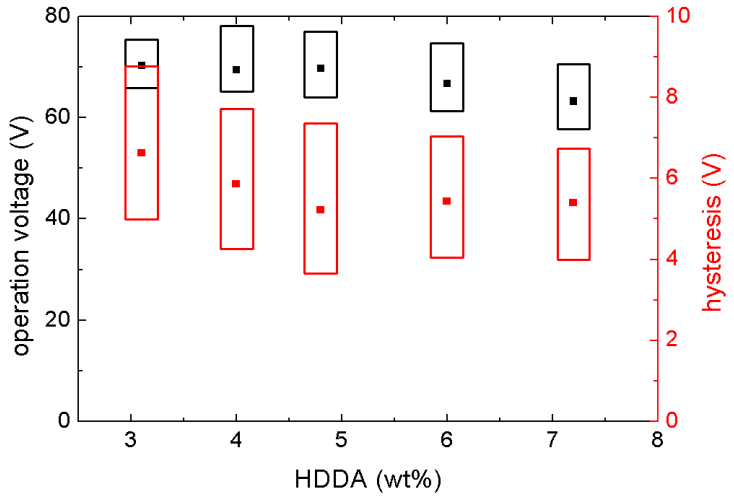

Figure 4.17.: Cross-linker fraction dependent operation voltage (black) and hysteresis (red) for mixtures containing HDDA and 12 wt% monomer in total. The bars indicate the range between the lowest and the highest value within a temperature range from 20 °C to 50 °C. Additionally, the mean value (square) is shown.

Considering the electro-optic measurements, the sample containing 4.8 wt% BPRM-1 and 7.2 wt% HDDA has the best performance. Its small variation of the hysteresis probably indicates a stiff polymer network. As discussed in literature [66], hysteresis may increase when the polymer network is deformed by an external electric field, which is prohibited in stiff polymer networks. The conversion of this mixture can also be interpreted as a result of a highly cross-linked and therefore stiff polymer network. The large amount of di-functional groups results in the high degree of cross-linking. Diffusion of the remaining monomers to the reactive sides is hindered and the reaction continues slowly as discussed in section 2.4.2. The heat induced by this slow reaction might be below the sensitivity of the photo-DSC instrument, which seems to signalize that the reaction is already terminated at lower conversion.

If the optimum ratio of BPRM-1 and HDDA is 2:3 as discussed in this section, the mixtures investigated in sections 4.2.1 and 4.2.2 with a ratio of 3:2 of mono- and di-functional monomer show no optimized performance. However, they provide reasonable stabilization of the BP structure to conduct experiments, where other aspects of the composition are investigated. It should be emphasized that the maximum fraction of cross-linker is limited in this study by reduction of the clearing temperature, which is caused by the non-mesogenic compound HDDA.

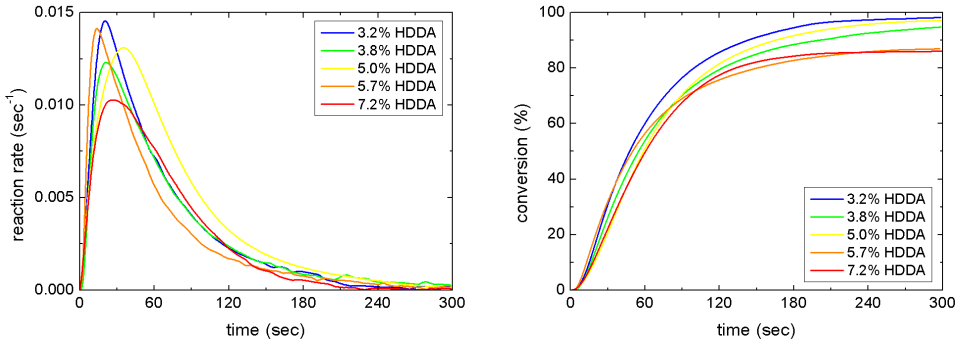

Figure 4.18.: Reaction rate (a) and conversion (b) for mixtures containing different fractions of HDDA.

4.2.4. Different kinds of cross-linkers

In this study, three different cross-linkers were used: the mesogenic di-acrylate BPRM-2, the non-mesogenic di-acrylate HDDA and the non-mesogenic di-methacrylate HDDMA. The corresponding BP mixtures are listed in tables A.8a to A.8c, respectively. They contain 6 wt% BPRM-1 and 4 wt% of the respective cross-linker. Phase transition and polymerization temperature are listed in table B.15. In fig. 4.19, the electro-optic performance for these three types of cross-linker is compared.

Operation voltage and hysteresis are shown in fig. 4.19a. The mixture containing the mesogenic cross-linker BPRM-2 requires a higher operation voltage than the other mixtures. Furthermore, the variation between the minimum and maximum value of the operation voltage within the investigated temperature range is much larger for BPRM-2 than for HDDA or HDDMA. The lowest operation voltage is observed when HDDA was used as cross-linker. The average value of the hysteresis is smallest when BPRM-2 is used as cross-linker and increases for HDDA and HDDMA. The variation of the hysteresis is larger in the mixture containing HDDA than in the other two mixtures.

The response times t_{on} and t_{off} (fig. 4.19b) are particularly small in the mixture with the mesogenic cross-linker. This mixture also exhibits the smallest temperature dependence of the response times. In the mixtures containing HDDA and HDDMA the temperature dependence is much larger, especially for the response time t_{off}. Since the extreme values largely deviate from the mean values, the mean values are plotted in a different way in fig. 4.20 for better comparability. The re-

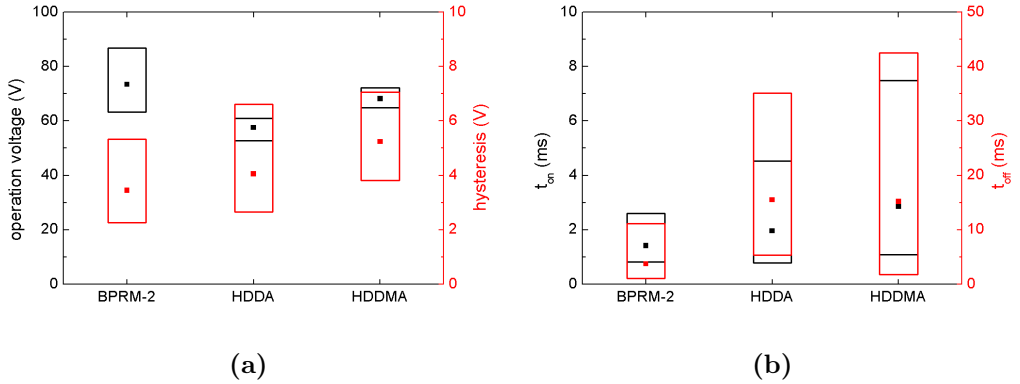

(a) **(b)**

Figure 4.19.: Cross-linker type dependent electro-optic performance for mixtures containing 6 wt% BPRM-1 and 4 wt% HDDA: (a) operation voltage (black) and hysteresis (red) and (b) response times t_{on} (black) and t_{off} (red). The bars indicate the range between the lowest and the highest value within a temperature range from 20 °C to 50 °C. Additionally, the mean value (square) is shown.

sponse time t_{on} of all mixtures was in the ms-range. However, a trend towards slower response times was observed when using the cross-linkers BPRM-2, HDDA and HDDMA, respectively. The fastest response time $t_{off} < 5$ ms was measured for the mixture with the mesogenic cross-linker BPRM-2, while $t_{off} \approx 15$ ms in the other mixtures with non-mesogenic cross-linkers.

For the mixtures compared above, the electro-optic performance was quite similar, but not identical, when HDDA and HDDMA were used as cross-linker. This indicates that a small modification of the molecule — the hydrogen in HDDA was substituted with a methyl group in HDDMA (fig. 3.2) — already influences the performance. Therefore, it is interesting to analyze and compare the performance of mixtures with different cross-linker fractions of HDDA (table A.7a) and HDDMA (table A.7b). The corresponding phase transition and polymerization temperatures are shown in table B.14. The results for these mixtures are depicted in fig. 4.21. The operation voltage of mixtures containing HDDA is lower than of those containing HDDMA. Most remarkable are the different trends for the operation voltage, which slightly decreases with increasing fraction of HDDA and increases with increasing fraction of HDDMA. The hysteresis is almost independent of the cross-linker fraction for both kinds of cross-linker. In general, hysteresis was larger when HDDMA was used as cross-linker.

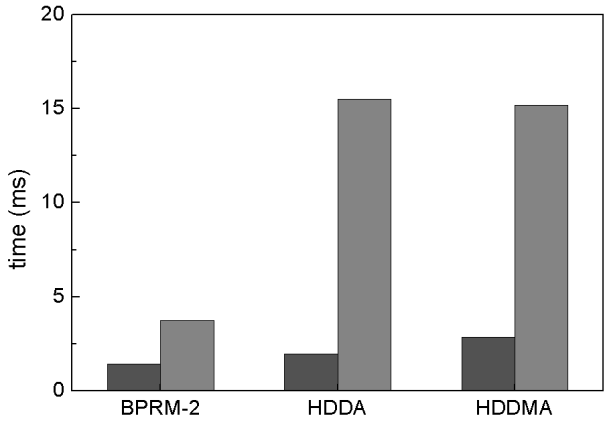

Figure 4.20.: Mean values of the response times t_{on} (dark gray) and t_{off} (gray) for mixtures containing different kinds of cross-linkers.

In addition to the electro-optic measurements, photo-DSC was used to analyze the conversion of the photo-polymerization. In fig. 4.22, the conversion is depicted for the same mixtures containing HDDA (green) or HDDMA (blue) as in fig. 4.21. The highest conversion for mixtures containing HDDA is observed for the mixture with a ratio 3:2 of mono- and di-functional monomers. In contrast, the conversion is highest for the mixture with the largest fraction of HDDMA.

When fig. 4.21 is compared to fig. 4.22, it is found that the electro-optic performance of mixtures containing HDDA as cross-linker does not directly depend on the conversion of the polymerization reaction. In contrast, the mixtures containing HDDMA require higher operation voltages and exhibit larger hysteresis when the conversion of the reaction is higher.

The different trends observed for the operation voltage of mixtures containing HDDA and HDDMA, respectively, indicate that the BP system always requires optimization of the composition when a substance is exchanged, regardless how similar the exchanged substances are.

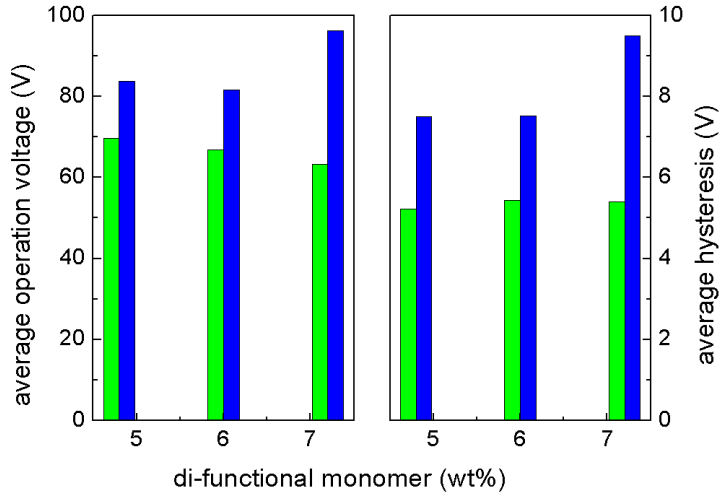

Figure 4.21.: Cross-linker type dependent mean values of operation voltage (left) and hysteresis (right) for mixtures containing 12 wt% monomers and varying fractions of HDDA (green) and HDDMA (blue), respectively. All mixtures were investigated in a temperature range from 20 °C to 50 °C.

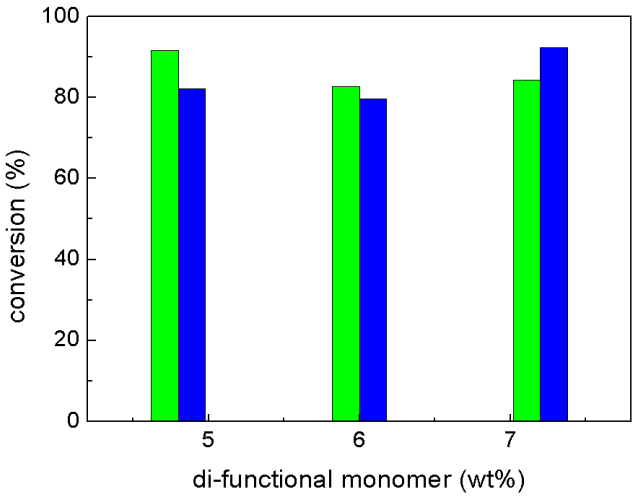

Figure 4.22.: Conversion of the polymerization reaction of mixtures containing the cross-linker HDDA (green) and HDDMA (blue).

4.2.5. Polymerization temperature

The BP structure existing at the polymerization temperature is stabilized by the polymer network. In literature [78], it was reported that the electro-optic performance of PSBP can differ for stabilization of BPI and BPII. For intentional stabilization of a specific BP modification, the phase sequence of the mixture needs to be known. The selective reflections of the investigated mixture 'HDDA' (table A.8b) were in the UV wavelength range so that it was impossible to observe the phase sequence directly by POM. In our previous study [70], we found that the electro-optic performance of mixtures containing no photo-curable substances (monomers, photo-initiator) is similar to the performance of unstabilized mixtures, which contain photo-curable substances. Therefore, it was tried to elucidate the phase sequence of the more simple mixture B (table A.2), which also contained 3.8 wt% of chiral dopant but no photo-curable substances.

The following approach was chosen to elucidate the phase sequence of a sample with high chirality and selective reflections in the UV wavelength range (mixture B). The curve of the temperature dependent Kerr constant of mixture B was compared to the curve of mixture A, the phase sequence of which was known (section 4.1.1): First, the phase sequence of mixture A obtained by optical spectroscopy is superimposed to the electro-optical data to assign the phase sequence as shown in fig. 4.23. In the next step, the electro-optical data of mixture A and

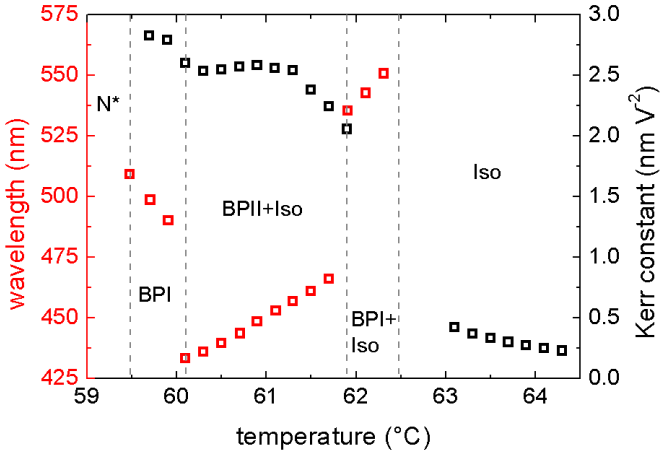

Figure 4.23.: Superposition of the temperature dependent Bragg reflections and Kerr constants of mixture A to assign the phase sequence to the electro-optically obtained data.

mixture B is compared (fig. 4.24). From this comparison of the temperature dependences $K(T)$, the presumable phase sequence of mixture B can be derived. The temperature ranges of the phases observed by POM and spectroscopy correspond to different slopes of the temperature dependent Kerr constant for mixture A as shown in fig. 4.24. Since the curve of the temperature dependent Kerr constant progresses similarly for both mixtures, the same phase sequence as in mixture A is supposed for mixture B.

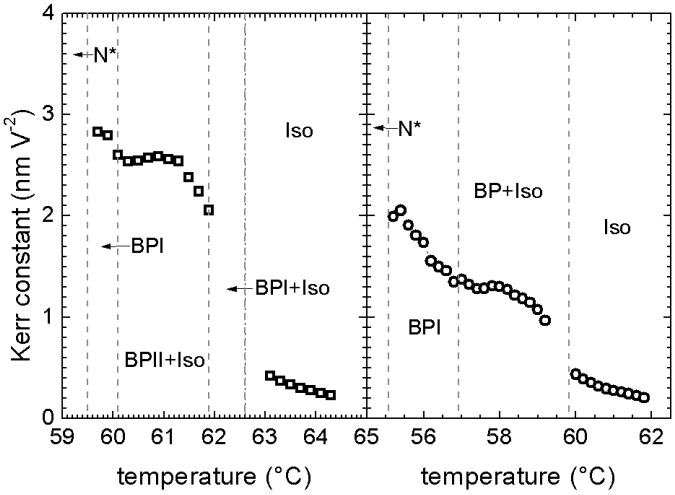

Figure 4.24.: Temperature dependent Kerr constants for mixture A (left) and mixture B (right) containing 2.8 wt% and 3.8 wt% of the chiral dopant, respectively. The phase sequence of mixture A is known. Based on the similar slopes of the curves, the phase sequence of mixture B was assigned.

The temperature dependent Kerr constants for different unstabilized samples containing mixture 'HDDA' are depicted in fig. 4.25. The vertical lines indicate the specific polymerization temperatures of the samples (table B.15). Minor deviations of the performance occur for the unstabilized samples. These can be attributed to slight variations of the cell thickness and non-ideal preparation conditions. In general, the curves progress as those in fig. 4.24 and the same phase sequence is supposed. The samples were heated during the electro-optic measurement of the unstabilized samples. Then, they were cooled down fast to the specific polymerization temperatures. Electro-optic measurements of the PSBP samples were performed subsequent to polymerization. The polymerization temperatures were chosen according to the phase sequence determined for the heated samples. When the samples were cooled fast, this may result in supercooling of BP and the

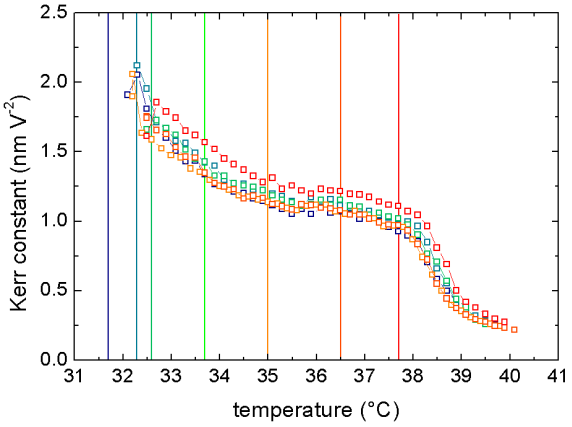

Figure 4.25.: Temperature dependent Kerr constants for unstabilized samples containing mixture 'HDDA'. Temperatures chosen for polymerization are indicated as lines, which are of the same color as the corresponding electro-optic measurement of the samples.

phase sequence might be different. Since no constant cooling rate was used, deviations from the phase sequence proposed for heating were unpredictable. Neglecting this possibility, the chosen polymerization temperatures include super-cooled BPI, BPI, BPII and the two-phase region, where BP and isotropic droplets coexist.

In fig. 4.26, the resulting operation voltage (black) and hysteresis (red) are shown. Both parameters are nearly unaffected by the polymerization temperature.

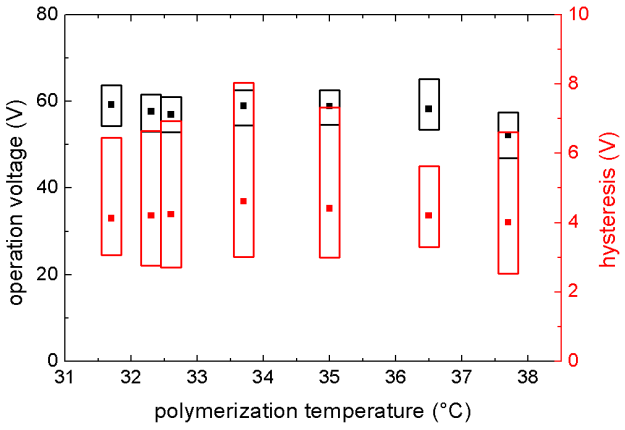

Figure 4.26.: Polymerization temperature dependent operation voltage (black) and hysteresis (red) for mixture 'HDDA'. The bars indicate the range between the lowest and the highest value within a temperature range from 20 °C to 50 °C. Additionally, the mean value (square) is shown.

Additionally, photo-DSC measurements were performed for different polymerization temperatures. The corresponding conversions of the polymerization reaction are shown in fig. 4.27. The conversion is similar for all polymerization temperatures.

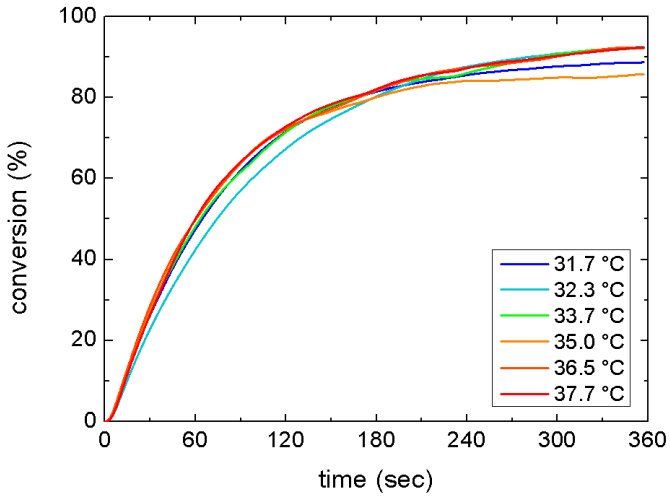

Figure 4.27.: Conversion of the photo-polymerization for different samples containing mixture 'HDDA'. The reaction was initiated at different temperatures.

Neither the polymerization reaction nor the electro-optic performance are significantly influenced by the polymerization temperature. This indicates that no precise temperature control is necessary to counteract heating effects caused by the UV light source. Nevertheless, it is advantageous to choose a low polymerization temperature to ensure polymerization in the BP range and avoid regions where BP and Iso coexist. Stabilization of co-existence regions reduces the Kerr constant of the sample, because K is much lower in the isotropic phase than in the BP. Different densities of both phases may also result in optical inhomogeneity of the sample.

4.2.6. UV exposure time

To obtain well-defined structures with reproducible properties, the sample should be illuminated until the polymerization reaction is finished. If the illumination is stopped before the polymerization reaction is finished, it is expected that the reaction proceeds slowly. In this case, the performance of the test cell would

change. The polymerization kinetics of mixture 'HDDA' were studied by photo-DSC. The reaction is complete after 5 min as depicted in fig. 4.28.

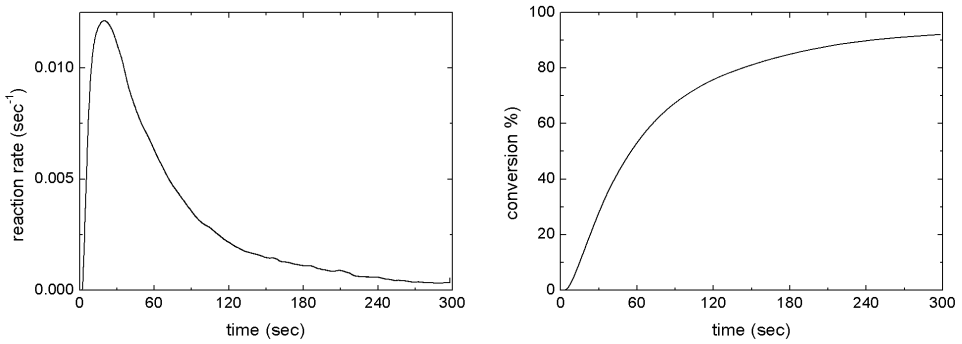

Figure 4.28.: Reaction rate (a) and conversion (b) of mixture 'HDDA'.

To test to which extent the UV exposure time affects the performance, four samples containing mixture 'HDDA' were investigated. The polymerization temperatures for the different cells are listed in table B.18. Each sample was illuminated for a different time period between 2 min and 5 min. The electro-optical results are shown in fig. 4.29. The operation voltage (black) and the hysteresis (red) were analyzed in a temperature range from 20 °C to 52 °C. Each sample was investigated two times: first directly after PSBP was generated (a) and again 5 days later (b). Comparing fig. 4.29a and fig. 4.29b, reveals a reduced range between minimum and maximum values of the hysteresis for illumination periods of 2 min and 3 min. To analyze smaller changes, the mean values of operation voltage (left) and hysteresis (right) are plotted in a bar diagram in fig. 4.30 for the first (dark gray) and the second (gray) measurement. This diagram confirms that the operation voltage and the hysteresis change significantly for 2 min and 3 min of UV exposure, where the illumination was interrupted before the maximum conversion was reached. The operation voltage increases and after some days it becomes equal to the operation voltage measured directly for the completely polymerized sample. After five days, the hysteresis for the completely stabilized sample is unchanged, but samples with incomplete stabilization have a reduced hysteresis compared to the first measurement. It is most likely that the polymerization proceeds slower without UV illuminations. Probably, the slower reaction rate supports diffusion of monomers and short polymer chains to the disclination lines before they were immobilized by cross-linking. Better separation of polymer and LC is expected to

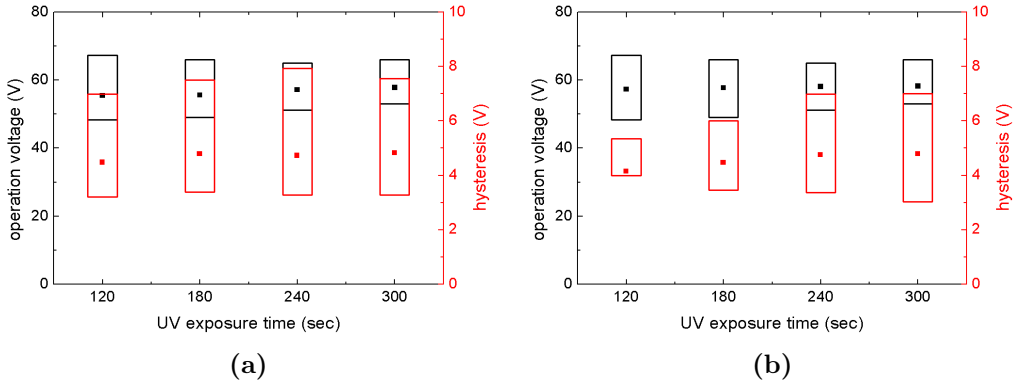

Figure 4.29.: UV exposure time dependent operation voltage (black) and hysteresis (red) for mixture 'HDDA' at the day of sample preparation (a) and five days later (b). The bars indicate the range between the lowest and the highest value within a temperature range from 20 °C to 52 °C. Additionally, the mean value (square) is shown.

reduce hysteresis as we observe it for the sample with an initial UV exposure time of 2 min.

According to these observations, the illumination period of 3 min with an intensity of 3 mW cm^{-2} stated in the preparation routine (section 3.2) is too short to acquire complete polymerization. The routine was developed at Merck KGaA Darmstadt, where the samples were illuminated with UV light of about 365 nm. Other wavelengths were cut off by a filter. In our setup no filter was used. Thus, more wavelength contribute to the illumination intensity, which was constant. Consequently, a longer exposure time is needed to illuminate the sample with the same dose of the wavelength, which is absorbed by the photo-initiator. On the other hand, interrupted illumination might be used intentionally to reduce the hysteresis of the sample. So far, it is not clear what happens during the resting period the sample requires to reach constant electro-optic performance.

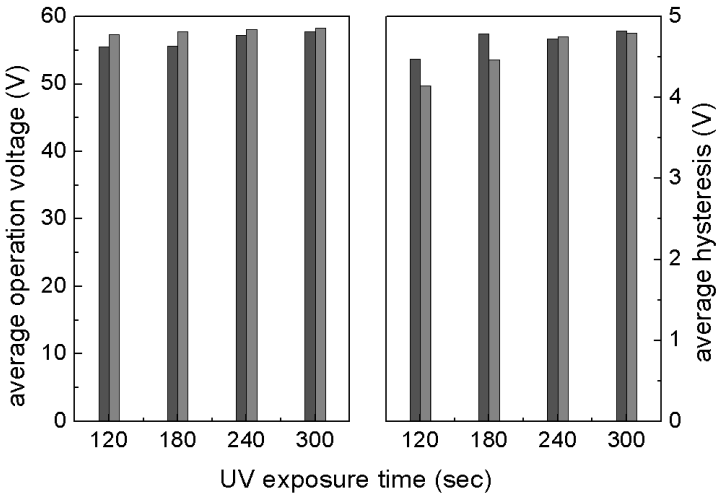

Figure 4.30.: UV exposure time dependent mean values of operation voltage (left) and hysteresis (right) compared for the day of preparation (dark gray) and five days later (gray), respectively.

5. Conclusions and Outlook

In this work, a variety of methods was used to study the performance of PSBPs, among them photo-DSC, which is not commonly used in this field of investigations. An important aspect of the electro-optic studies is the systematic investigation of the performance over broad temperature ranges, which is in contrast to many publications, where only the performance at a specific temperature (often RT) is presented. The research was focused on two aspects: first the general properties of blue phase stabilization were characterized, the second step included systematic variations of substance composition and polymerization conditions with the goal to optimize the electro-optic performance. A distinct feature of this work are the used monomers. For the basic experiments on polymer-stabilization effects, both mono- and di-functional monomers were mesogenic. For the systematic variation of the sample composition, mesogenic mono-functional monomers and non-mesogenic cross-linkers were used, complementary to current studies by other researchers.

The basic studies described in the first part (section 4.1) were enabled by observing Bragg reflections in the visible wavelength range, which proved to be a very valuable tool for this kind of study. With POM and spectroscopy the phase sequence of pure BP and PSBP samples was determined. With the help of dynamic electro-optic characterization, it was found that slow effects like electrostriction and field-induced phase transitions are suppressed in PSBPs. This enables faster switching, which is important for a wide range of applications including color sequential displays and 3D movies. In this context, a fast and easy method to judge the stability of BPs with visible Bragg reflections was established: good polymer-stabilization is achieved, when always the same platelet texture is observed in PSBP, even before and after a phase transition to the isotropic or cholesteric phase is induced by thermal or electrical treatment.

In the second part, mixtures with higher chirality were studied, so that Bragg reflections moved to the UV wavelength range, which is essential for display applications. It was shown, that similar to more common PSBPs, these systems

require higher operation voltages. The variation of the monomer fraction shows that trade-offs between operation voltage and hysteresis are necessary. Overall, the performance is robust against changes of the monomer fraction in the investigated range from 8 wt% to 12 wt%. When varying the fraction of HDDA, the highest studied fraction of HDDA to BPRM-1 of 3:2 shows the best electro-optic results. Comparison of the different cross-linker types indicates that the operation voltage is reduced by using a non-mesogenic cross-linker at the expense of slower response times. The electro-optic performance of mixtures containing either HDDA or HDDMA is quite similar for some sample compositions, but variations of the cross-linker fraction indicate that the optimum performance is not achieved for the same ratio of mono- and di-functional monomers. The sensitivity of the system to small variations of the composition demonstrates how important optimization of the composition is for the specific substances.

Concerning the preparation conditions, one can conclude that the performance is independent of the polymerization temperature as long as stabilization takes place in the blue phase. The time of UV exposure needed for complete stabilization of a mixture with a certain illumination intensity was determined using photo-DSC. According to the electro-optic results, the polymerization reaction proceeds further after incomplete UV polymerization. Surprisingly, in those samples, where the illumination was terminated early, a lower hysteresis appears.

In summary, combining mesogenic mono-functional monomers with non-mesogenic cross-linkers is as an alternative to previously studied systems when creating PSBPs: Both systems have a similar electro-optic performance and similar trends known from other systems were observed in the new system, such as increasing operation voltage with increasing amount of the chiral dopant. The results show that this new material combination is promising. However, there is room for further chemical improvement of the substances.

Basic understanding of BPs containing a new nematic host and a new monomer composition was established in this thesis. To complete the information on phase sequences, electrostriction and field-induced phase transitions, Kossel measurements are suggested. They enable analysis of field-induced BP modifications and allow determination of lattice orientations in BP platelets. Regarding further optimization, the response times of our mixtures need further attention. They are in the ms-range rather than in the µs-range because the LC host material is highly viscous. Improvement is expected when a diluter is added to our mixtures. The positive effect of a diluter on the response times has already been demonstrated

for other BP mixtures containing a LC host with high viscosity [79]. This thesis was focused on studying the influence of chemical composition for a novel PSBP system, but it should be emphasized that the performance of this system can easily be further improved by optimizing also the technical boundary conditions, such as the device geometry.

Appendix

A. Sample compositions

The samples below were prepared according to the preparation process described in section 3.2.1. They are categorized with respect to the purpose and the appearance in the thesis. First, the composition of individual mixtures without monomer content (appendix A.1) is given, succeeded by the composition of individual mixtures with monomer content (appendix A.2). Then the composition of mixtures used for test series is included starting with polymerizable mixtures in appendix A.3. Finally, the composition of an additional test series for mixtures without monomer content is shown in appendix A.4.

A.1. BP mixtures without monomers

Table A.1.: Composition of mixture A.

component	**substance**	$\chi_{\mathbf{w}}$ **(wt%)**
nematic LC	MDA-PB-3	97.21
chiral dopant	R5011	2.79

Table A.2.: Composition of mixture B.

component	**substance**	$\chi_{\mathbf{w}}$ **(wt%)**
nematic LC	MDA-PB-3	96.20
chiral dopant	R5011	3.80

A.2. PSBP mixtures with monomers

Table A.3.: Composition of mixture 1. This mixture was prepared at Merck Darmstadt by Dr. David Wilkes.

component	**substance**	$\chi_{\mathbf{w}}$ **(wt%)**
nematic LC	MDA-PB-3	87.00
chiral dopant	R5011	2.80
mono-functional monomer	BPRM-1	6.00
di-functional monomer	BPRM-2	4.00
photo-initiator	IRG 651	0.20

Table A.4.: Composition of mixture 2.

component	**substance**	$\chi_{\mathbf{w}}$ **(wt%)**
nematic LC	MDA-PB-3	86.01
chiral dopant	R5011	3.80
mono-functional monomer	BPRM-1	6.02
di-functional monomer	HDDMA	3.97
photo-initiator	IRG 651	0.21

A.3. PSBP mixtures for the test series with varying sample composition

Table A.5.: Composition of the mixtures (M) of test series 1 (TS1) with varying chirality. The amount of the substances is given in wt%.

mixture	MDA-PB-3	R5011	BPRM-1	HDDA	IRG 651
TS1M1	87.00	2.82	6.02	3.96	0.21
TS1M2	86.85	2.96	5.97	3.96	0.27
TS1M3	86.24	3.32	6.03	4.20	0.21
TS1M4	86.36	3.50	6.24	3.67	0.23
TS1M5	86.10	3.79	5.97	3.95	0.20

Table A.6.: Composition of the mixtures (M) of test series 2 (TS2) with varying monomer fraction. The amount of the substances is given in wt%.

mixture	MDA-PB-3	R5011	BPRM-1	HDDA	IRG 651
TS2M1	87.93	3.78	4.80	3.28	0.20
TS2M2	86.57	3.78	5.34	4.10	0.21
TS2M3	85.08	3.78	6.58	4.36	0.21
TS2M4	84.02	3.78	7.23	4.76	0.21

Table A.7.: Composition of the mixtures (M) of test series 3 (TS3) with varying amount of the cross-linker. As cross-linker HDDA (a) or HDDMA (b) were used. The amount of the substances is given in wt%.

mixture	MDA-PB-3	R5011	BPRM-1	HDDA	IRG 651
TS3M1	83.75	3.79	8.91	3.22	0.33
TS3M2	84.24	3.80	7.95	3.77	0.24
TS3M3	83.72	3.78	7.21	5.04	0.25
TS3M4	84.52	3.78	5.80	5.67	0.23
TS3M5	83.91	3.78	4.78	7.22	0.32

(a)

mixture	MDA-PB-3	R5011	BPRM-1	HDDMA	IRG 651
TS3M6	84.21	3.78	7.08	4.70	0.22
TS3M7	84.36	3.81	5.84	5.79	0.19
TS3M8	83.79	3.81	4.82	7.27	0.31

(b)

Table A.8.: Composition of the mixtures with different kinds of cross-linker. As cross-linker BPRM-1 (a), HDDA (b) and HDDMA (c) were used, respectively. The amount of the substances is given in wt%.

component	**substance**	$\chi_{\mathbf{w}}$ **(wt%)**
nematic LC	MDA-PB-3	85.10
chiral dopant	R5011	3.75
mono-functional monomer	BPRM-1	6.81
di-functional monomer	BPRM-2	3.95
photo-initiator	IRG 651	0.38

(a)

component	**substance**	$\chi_{\mathbf{w}}$ **(wt%)**
nematic LC	MDA-PB-3	86.10
chiral dopant	R5011	3.79
mono-functional monomer	BPRM-1	5.97
di-functional monomer	HDDA	3.95
photo-initiator	IRG 651	0.20

(b)

component	**substance**	$\chi_{\mathbf{w}}$ **(wt%)**
nematic LC	MDA-PB-3	86.01
chiral dopant	R5011	3.80
mono-functional monomer	BPRM-1	6.02
di-functional monomer	HDDMA	3.97
photo-initiator	IRG 651	0.21

(c)

A.4. Mixture without monomers for test series with varying sample composition

Table A.9.: Composition of the mixtures (M) of test series 1.0 (TS1.0) with varying chirality. The amount of the substances is given in wt%.

mixture	MDA-PB-3	R5011
TS1.0M1	97.49	2.51
TS1.0M2	97.21	2.79
TS1.0M3	96.91	3.09
TS1.0M4	96.49	3.51
TS1.0M5	96.20	3.80
TS1.0M6	95.80	4.20

B. Phase sequence and polymerization temperature of the mixtures

The phase sequence of the mixtures, whose composition is given in appendix A, was determined according to the procedure described in section 3.2.2. For samples with selective reflections in the UV wavelength range, only the N^* to BP transition can be determined by POM. Here, the phase sequences and the corresponding polymerization temperatures of pure BP mixtures and unstabilized PSBP mixtures are stated starting with the individual mixtures in appendix B.1 and continuing with the mixtures prepared for test series with (appendix B.2) and without monomer content (appendix B.3).

B.1. Individual mixtures

Table B.10.: Phase sequence of the mixtures without monomers. The phase sequence A' appears in cells with planar alignment.

mixture	**phase sequence** (°C)
A	N^* 59.47 BPI 60.10 BPII/Iso 61.88 BPI/Iso 62.50 Iso
A'	N^* 59.49 BPI 60.09 BPII 61.90 BPI/BPII/Iso 62.40 BPI/Iso 62.60 Iso
B	N^* 55.39 BP

Table B.11.: Phase sequence and polymerization temperature of the mixtures with monomers.

mixture	**phase transition** (°C)	$T_{\mathbf{poly}}$ (°C)
1	N^* 41.27 BP	41.76
2	N^* 27.45 BP	27.96

B.2. Mixtures for test series with monomer

Table B.12.: Phase sequence and polymerization temperature of the mixtures (M) of test series 1 (TS1) with varying chirality.

mixture	**phase transition** (°C)	$T_{\mathbf{poly}}$ (°C)
TS1M1	N^* 31.66 BP	32.16
TS1M2	N^* 30.06 BP	30.56
TS1M3	N^* 27.66 BP	28.16
TS1M4	N^* 28.85 BP	29.35
TS1M5	N^* 25.08 BP	25.67

Table B.13.: Phase sequence and polymerization temperature of the mixtures (M) of test series 2 (TS2) with varying monomer fraction.

mixture	**phase transition** (°C)	$T_{\mathbf{poly}}$ (°C)
TS2M1	N^* 31.26 BP	31.76
TS2M2	N^* 27.25 BP	27.75
TS2M3	N^* 24.66 BP	25.15
TS2M4	N^* 21.24 BP	21.75

Table B.14.: Phase sequence and polymerization temperature of the mixtures (M) of test series 3 (TS3) with varying amount of the cross-linker HDDA (a) or HDDMA (b).

mixture	**phase transition** (°C)	$T_{\mathbf{poly}}$ (°C)
TS3M1	N* 26.66 BP	27.15
TS3M2	N* 26.66 BP	27.16
TS3M3	N* 21.01 BP	21.51
TS3M4	N* 24.67 BP	25.20
TS3M5	N* 16.84 BP	17.35

(a)

mixture	**phase transition** (°C)	$T_{\mathbf{poly}}$ (°C)
TS3M6	N* 19.24 BP	19.74
TS3M7	N* 18.45 BP	18.95
TS3M8	N* 6.21 BP	6.74

(b)

Table B.15.: Phase sequence and polymerization temperature of the mixtures with different kinds of cross-linker BPRM-1, HDDA and HDDMA from table A.8.

cross-linker	**phase transition** (°C)	$T_{\mathbf{poly}}$ (°C)
BPRM-2	N* 41.27 BP	41.76
HDDA	N* 32.14 BP	32.66
HDDMA	N* 27.45 BP	27.96

B.3. Mixture for test series without monomers

Table B.16.: Phase sequence and polymerization temperature of the mixtures (M) of test series 1.0 (TS1.0) with varying chirality.

mixture	**phase sequence** (°C)
TS1.0M1	N^* 62.28 BPI 62.70 BPI/Iso 64.70 Iso
TS1.0M2	N^* 59.47 BPI 60.10 BPII/Iso 61.88 BPI/Iso 62.50 Iso
TS1.0M3	N^* 59.59 BP
TS1.0M4	N^* 59.28 BP
TS1.0M5	N^* 55.39 BP
TS1.0M6	N^* 53.30 BP

B.4. Cells to test preparation conditions

Table B.17.: Phase sequence and polymerization temperature of mixture 'HDDA' (tables A.8b and B.15) in the cells used to investigate the polymerization temperature.

cell	**phase transition** (°C)	$T_{\mathbf{poly}}$ (°C)
1	N^* 32.30 BP	31.70
2	N^* 32.10 BP	32.30
3	N^* 32.30 BP	32.60
4	N^* 32.70 BP	33.70
5	N^* 31.85 BP	34.96
6	N^* 32.27 BP	36.48
7	N^* 32.50 BP	37.70

Table B.18.: Phase sequence and polymerization temperature of mixture 'HDDA' (tables A.8b and B.15) in the cells used to investigate the UV exposure time.

cell	**exposure** (min)	**phase transition** (°C)	$T_{\mathbf{poly}}$ (°C)
1	2	N* 33.26 BP	33.75
2	3	N* 33.27 BP	33.76
3	4	N* 33.45 BP	33.96
4	5	N* 33.47 BP	33.97

C. Contributions in peer-reviewed journals

G. Nordendorf, A. Hoischen, J. Schmidtke, D. Wilkes, H.-S. Kitzerow, "Polymer-stabilized blue phases: promising mesophases for a new generation of liquid crystal displays", *Polym. Adv. Technol.* 25, 1195–1207 (2014)

G. Nordendorf, A. Lorenz, A. Hoischen, J. Schmidtke, H.-S. Kitzerow, D. Wilkes, M. Wittek, "Hysteresis and memory factor of the Kerr effect in blue phases", *J. Appl. Phys.* 114, 173104 (2013)

D. Conference contributions

D.1. Oral presentations[1]

G. Nordendorf, H.-S. Kitzerow, D. Wilkes, E. Plummer, "How blue phases benefit from polymer-stabilization", 21st Merck CASE Conference, Southampton UK (April 13–14, 2015)

G. Nordendorf, A. Hoischen, H.-S. Kitzerow, D. WIlkes, E. Plummer, "Performance of a polymer-stabilized blue phase from mesogenic mono-functional and non-mesogenic di-functional monomers", 42th German Liquid Crystal Conference, Stuttgart (March 4–6, 2015)

[1] presenting author underlined

G. Nordendorf, A. Hoischen, J. Schmidtke, D. Wilkes, M. Wittek, H.-S. Kitzerow, "Polymer-stabilized blue phases: Influence of a non-mesogenic cross-linker on the stabilization", 12$^{\text{th}}$ International Conference polymers for advanced technologies 2013, Berlin (September 29–October 2, 2013)

G. Nordendorf, A. Lorenz, A. Hoischen, J. Schmidtke, H.-S. Kitzerow, D. Wilkes, M. Wittek, "Hysteresis of the Kerr effect in Blue Phases", International Liquid Crystal Conference 2012, Mainz (August 19–24, 2012)

D.2. Poster presentations[1]

G. Nordendorf, A. Hoischen, J. Schmidtke, H.-S. Kitzerow, D. Wilkes, E. Plummer, "Influence of alignment layers on the electro-otic properties of blue phase liquid crystal cells", International Liquid Crystal Conference 2014, Dublin (June 29–July 4, 2014)

J. Schmidtke, G. Nordendorf, A. Lorenz, A. Hoischen, H.-S. Kitzerow, D. Wilkes, M. Wittek, "Exploring the phase diagram of UV reflecting blue phase systems", 40$^{\text{th}}$ Topical Meeting on Liquid Crystals, Paderborn (March 20–22, 2013)

G. Nordendorf, A. Hoischen, J. Schmidtke, D. Wilkes, M. Wittek, H.-S. Kitzerow, "Polymer-stabilized blue phases: effect of composition", 40$^{\text{th}}$ Topical Meeting on Liquid Crystals, Paderborn (March 20–22, 2013)

Bibliography

1. Reinitzer, F. Beiträge zur Kenntniss des Cholesterins. *Monatshefte für Chemie* **9,** 421–441 (1888).
2. Lehmann, O. Stoffe mit drei flüssigen Zuständen, einem isotropen und zwei kristallinisch-flüssigen. *Z. Phys. Chem.* **56,** 750 (1906).
3. Stegemeyer, H., Blümel, T., Hiltrop, K., Onusseit, H. & Porsch, F. Thermodynamic, structural and morphological studies on liquid-crystalline blue phases. *Liq. Cryst.* **1,** 3–28 (1986).
4. Kitzerow, H.-S. *et al.* Observation of blue phases in chiral networks. *Liq. Cryst.* **14,** 911–916 (1993).
5. Kikuchi, H., Yokota, M., Hisakado, Y., Yang, H. & Kajiyama, T. Polymer-stabilized liquid crystal blue phases. *Nat. Mater.* **1,** 64–68 (2002).
6. Jákli, A. *et al.* Reversible Switching Between Optically Isotropic and Birefringent States in a Bent-Core Liquid Crystal. *Adv. Mater.* **15,** 1606–1610 (2003).
7. Coles, H. J. & Pivnenko, M. N. Liquid crystal 'blue phases' with a wide temperature range. *Nature* **436,** 997–1000 (2005).
8. Yoshida, H. *et al.* Nanoparticle-Stabilized Cholesteric Blue Phases. *Appl. Phys. Express* **2,** 121501 (2009).
9. Ge, Z., Gauza, S., Jiao, M., Xianyu, H. & Wu, S.-T. Electro-optics of polymer-stabilized blue phase liquid crystal displays. *Appl. Phys. Lett.* **94,** 101104 (2009).
10. Gray, G., Harrison, K. & Nash, J. New family of nematic liquid crystals for displays. *Electron. Lett.* **9,** 130–131 (1973).
11. Eidenschink, R., Erdmann, D., Krause, J. & Pohl, L. Substituierte Phenylcyclohexane – eine neue Klasse flüssigkristalliner Verbindungen. *Angew. Chem.* **89,** 103–103 (1977).

12. Nordendorf, G., Hoischen, A., Schmidtke, J., Wilkes, D. & Kitzerow, H.-S. Polymer-stabilized blue phases: promising mesophases for a new generation of liquid crystal displays. *Polym. Adv. Technol.* **25,** 1195–1207 (2014).

13. Gennes, P. G. d. & Prost, J. *The Physics of Liquid Crystals* Second Edition. 616 pp. (Clarendon Press — International Series of Monographs on Physics 83, 1995).

14. Dubois-violette, E. & Pansu, B. Frustration and Related Topology of Blue Phases. *Mol. Cryst. Liq. Cryst. Incorp. Nonlin. Optics* **165,** 151–182 (1988).

15. *Nematic and chiral nematic liquid crystals* (eds Goodby, J. W. *et al.*) second edition. 8 vols. (Wiley-VCH, 2014).

16. Johnson, D. L., Flack, J. H. & Crooker, P. P. Structure and Properties of the Cholesteric Blue Phases. *Phys. Rev. Lett.* **45,** 641–644 (1980).

17. Hornreich, R. & Shtrikman, S. Optical selection rules and structures of cholesteric blue phases. *Phys. Lett. A* **82,** 345–349 (1981).

18. *Chirality in Liquid Crystals* (eds Kitzerow, H.-S. & Bahr, C.) (Springer-Verlag, New York, 2001).

19. Flack, J. H. & Crooker, P. P. Polarization and pitch dependence of cholesteric blue-phase structures. *Phys. Lett. A* **82,** 247–250 (1981).

20. Rao, L., Yan, J., Wu, S.-T., Yamamoto, S.-i. & Haseba, Y. A large Kerr constant polymer-stabilized blue phase liquid crystal. *Appl. Phys. Lett.* **98,** 081109 (2011).

21. Gerber, P. R. Electro-Optical Effects of a Small-Pitch Blue-Phase System. *Mol. Cryst. Liq. Cryst.* **116,** 197–206 (1985).

22. Yan, J. *et al.* Low voltage and high contrast blue phase liquid crystal with red-shifted Bragg reflection. *Appl. Phys. Lett.* **102,** 011113 (2013).

23. Chen, Y. *et al.* A microsecond-response polymer-stabilized blue phase liquid crystal. *Appl. Phys. Lett.* **99,** 201105 (2011).

24. Chen, K.-M., Gauza, S., Xianyu, H. & Wu, S.-T. Submillisecond Gray-Level Response Time of a Polymer-Stabilized Blue-Phase Liquid Crystal. *J. Display Technol.* **6,** 49–51 (2010).

25. Xu, D. *et al.* Electro-optic response of polymer-stabilized blue phase liquid crystals. *Appl. Phys. Lett.* **105,** 011119 (2014).

26. Heppke, G., Kitzerow, H.-S. & Krumrey, M. Angular Dependence of Blue Phase Selective Reflection in the Electric Field. *Mol. Cryst. Liq. Cryst. Incorp. Nonlin. Optics* **150,** 265–276 (1987).

27. Kitzerow, H. S. The Effect of Electric Fields on Blue Phases. *Mol. Cryst. Liq. Cryst.* **202,** 51–83 (1991).

28. Cladis, P. E., Garel, T. & Pieranski, P. Kossel Diagrams Show Electric-Field-Induced Cubic-Tetragonal Structural Transition in Frustrated Liquid-Crystal Blue Phases. *Phys. Rev. Lett.* **57,** 2841–2844 (1986).

29. Pieranski, P. & Cladis, P. E. Field-induced tetragonal blue phase (BP X). *Phys. Rev. A* **35,** 355–364 (1987).

30. Pieranski, P., Cladis, P. & Barbet-Massin, R. Experimental evidence for a hexagonal Blue Phase. *J. Phys. Lett.* **46,** 973–977 (1985).

31. Heppke, G., Jéròme, B., Kitzerow, H.-S. & Pieranski, P. Observation of a hexagonal blue phase in systems with negative dielectric anisotropy. *Liq. Cryst.* **5,** 813–828. ISSN: 0267-8292 (1989).

32. Hornreich, R. M. & Shtrikman, S. Field-induced hexagonal blue phases in positive and negative dielectric anisotropy systems: Phase diagrams and topological properties. *Phys. Rev. A* **41,** 1978–1989 (1990).

33. Coles, H. J. & Gleeson, H. F. Electric Field Induced Phase Transitions and Colour Switching in the Blue Phases of Chiral Nematic Liquid Crystals. *Mol. Cryst. Liq. Cryst.* **167,** 213–225 (1989).

34. Schadt, M. & Helfrich, W. VOLTAGE-DEPENDENT OPTICAL ACTIVITY OF A TWISTED NEMATIC LIQUID CRYSTAL. *Appl. Phys. Lett.* **18,** 127–128 (1971).

35. Schadt, M. Milestone in the History of Field-Effect Liquid Crystal Displays and Materials. *Jpn. J. Appl. Phys.* **48,** 03B001 (2009).

36. *VA-Technologie für LC-Displays* <`http://www.merck-performance-materials.com/de/display/function_of_lcd_technology/va/va.html`> (2015).

37. Rao, L. *et al.* Critical Field for a Hysteresis-Free BPLC Device. *J. Display Technol.* **7,** 627–629 (2011).

38. Ge, Z., Rao, L., Gauza, S. & Wu, S.-T. Modeling of Blue Phase Liquid Crystal Displays. *J. Display Technol.* **5,** 250–256 (2009).

39. Xu, D., Chen, Y., Liu, Y. & Wu, S.-T. Refraction effect in an in-plane-switching blue phase liquid crystal cell. *Opt. Express* **21,** 24721–24735 (2013).

40. Chen, Y., Xu, D., Wu, S.-T., Yamamoto, S.-i. & Haseba, Y. A low voltage and submillisecond-response polymer-stabilized blue phase liquid crystal. *Appl. Phys. Lett.* **102,** 141116 (2013).

41. Lan, Y.-F. *et al.* Non-ideal optical isotropy of blue phase liquid crystal. *Appl. Phys. Lett.* **105,** 011903 (2014).

42. Flory, P. J. *Principles of Polymer Chemistry* 688 pp. (Cornell University Press, Ithaca, NY, 1953).

43. Carothers, W. H. STUDIES ON POLYMERIZATION AND RING FORMATION. I. AN INTRODUCTION TO THE GENERAL THEORY OF CONDENSATION POLYMERS. *J. Am. Chem. Soc.* **51,** 2548–2559 (1929).

44. Hiemenz, P. C. *Polymer chemistry - The basic concepts* 738 pp. (Marcel Dekker, Inc., New York, 1984).

45. Sandner, M. R. & Osborn, C. L. Photochemistry of 2,2-dimethoy-2-phenyl-acetophenone-triplet detection via "spin memory". *Tetrahedron Lett.* **15,** 415–418 (1974).

46. Groenenbook, C. J., Hageman, H. J., Overeem, T. & Weber, A. J. M. Photoinitiators and photoinitiation, 3. Comparison of the photodecompositions of α-methoxy- and α,α-dimethoxydeoxybenzoin in 1,1-diphenylethylene as model substrate. *Makromol. Chem.* **183,** 281–292 (1982).

47. Kaczmarek, H. Effect of Irgacure 651 Initiator on Poly(Methyl Methacrylate) Photostability Studied by UV-Vis Spectroscopy. *Open Process Chemistry Journal* **1,** 8–11 (June 24, 2013).

48. Trommsdorff, V. E., Köhle, H. & Lagally, P. Zur Polymerisation des Methacrylsäuremethylesters 1. *Makromol. Chem.* **1,** 169–198 (1948).

49. Hoischen, A. *Untersuchungen an photo-reaktiven Flüssigkristallsystemen* Dissertation (Universität Paderborn, Paderborn, 2005).

50. Lee, M. *et al.* Liquid crystalline blue phase I observed for a bent-core molecule and its electro-optical performance. *J. Mater. Chem.* **20,** 5813–5816 (2010).

51. Taushanoff, S. *et al.* Stable amorphous blue phase of bent-core nematic liquid crystals doped with a chiral material. *J. Mater. Chem.* **20,** 5893–5898 (2010).

52. Aya, S. *et al.* Stable electro-optic response in wide-temperature blue phases realized in chiral asymmetric bent dimers [Invited]. *Opt. Mater. Express* **4,** 662–671 (2014).

53. He, W. *et al.* Wide Blue Phase Range in a Hydrogen-Bonded Self-Assembled Complex of Chiral Fluoro-Substituted Benzoic Acid and Pyridine Derivative. *Adv. Mater.* **21,** 2050–2053 (2009).

54. Kasch, N., Dierking, I. & Turner, M. Stabilization of the liquid crystalline blue phase by the addition of short-chain polystyrene. *Soft Matter* **9,** 4789–4793 (2013).

55. Karatairi, E. *et al.* Nanoparticle-induced widening of the temperature range of liquid-crystalline blue phases. *Phys. Rev. E Stat. Nonlin. Soft. Matter Phys.* **81,** 041703 (2010).

56. Rožič, B. *et al.* Theoretical and experimental study of the nanoparticle-driven blue phase stabilisation. *Eur. Phys. J. E* **34,** 1–11 (2011).

57. Sharma, A., Worden, M. & Hegmann, T. Nanoparticle-Promoted Thermal Stabilization of Room Temperature Cholesteric Blue Phase Mixtures. *Ferroelectrics* **431,** 154–163 (2012).

58. Wang, L. *et al.* Hysteresis-Free Blue Phase Liquid-Crystal-Stabilized by ZnS Nanoparticles. *Small* **8,** 2189–2193 (2012).

59. Wang, L. *et al.* Low voltage and hysteresis-free blue phase liquid crystal dispersed by ferroelectric nanoparticles. *J. Mater. Chem.* **22,** 19629–19633 (2012).

60. Iwata, T. *et al.* Control of Cross-Linking Polymerization Kinetics and Polymer Aggregated Structure in Polymer-Stabilized Liquid Crystalline Blue Phases. *Macromolecules* **42,** 2002–2008 (2009).

61. Higashiguchi, K., Yasui, K. & Kikuchi, H. Direct Observation of Polymer-Stabilized Blue Phase I Structure with Confocal Laser Scanning Microscope. *J. Am. Chem. Soc.* **130,** 6326–6327 (2008).

62. Hussain, Z. *et al.* Effect of long flexible chain reactive monomers on the operating voltage of optically isotropic blue phase liquid crystals. *Liq. Cryst.* **39,** 221–230 (2012).

63. Chen, Y. & Wu, S.-T. Recent advances on polymer-stabilized blue phase liquid crystal materials and devices. *J. Appl. Polym. Sci.* **131,** 40556 (2014).

64. Iwata, T., Suzuki, K., Higuchi, H. & Kikuchi, H. A method for enlarging the Kerr constant of polymer-stabilised blue phases. *Liq. Cryst.* **36,** 947–951 (2009).

65. Choi, H., Higuchi, H., Ogawa, Y. & Kikuchi, H. Polymer-stabilized supercooled blue phase. *Appl. Phys. Lett.* **101,** 131904 (2012).

66. Lan, Y.-F., Tsai, C.-Y., Lu, J.-K. & Sugiura, N. Mechanism of hysteresis in polymer-network stabilized blue phase liquid crystal. *Polymer* **54,** 1876–1879 (2013).

67. Liu, Y. *et al.* A hysteresis-free polymer-stabilised blue-phase liquid crystal. *Liq. Cryst.* **41,** 1339–1344 (2014).

68. Xu, D., Yuan, J., Schadt, M. & Wu, S.-T. Blue phase liquid crystals stabilized by linear photo-polymerization. *Appl. Phys. Lett.* **105,** 081114 (2014).

69. Carbone, G. *et al.* Short pitch cholesteric electro-optical device based on periodic polymer structures. *Appl. Phys. Lett.* **95,** 011102 (2009).

70. Nordendorf, G. *et al.* Hysteresis and memory factor of the Kerr effect in blue phases. *J. Appl. Phys.* **114,** 173104 (2013).

71. Ciba Specialty Chemicals Inc. *Ciba® IRGACURE® 651*

72. *Dr. Hoenle UV-Technologie* <`http://www.hoenle.de/uv-produkte/uv-geraete-bluepoint/uv-haertung-bluepoint-4-easycure/`> (2015).

73. Wittek, M. *et al.* 4.4: New Materials for Polymer-Stabilized Blue Phase. *SID Symp. Dig. Tech. Papers* **43,** 25–28 (2012).

74. Ghorpade, R. V. *et al.* Photopolymerization kinetics of 2-phenylethyl (meth)-acrylates studied by photo DSC. *J. Polym. Res.* **19,** 1–8 (2012).

75. Marcus, M. A. Possible Non-Existence of "Blue Phase IIB". *Mol. Cryst. Liq. Cryst.* **82,** 33–39. ISSN: 0026-8941 (1982).

76. Nordendorf, G. *Electro-optic characterisation of polymer-stabilised liquid crystal blue phases* Master thesis (Universität Paderborn, Paderborn, 2012).

77. Nayek, P. *et al.* Tailoring Monodomain in Blue Phase Liquid Crystal by Surface Pinning Effect. **5,** 051701 (2012).

78. Choi, H., Higuchi, H. & Kikuchi, H. Fast electro-optic switching in liquid crystal blue phase II. **98,** 131905 (2011).

79. Chen, Y. *et al.* Diluter Effects on Polymer-Stabilized Blue Phase Liquid Crystals. *J. Display Technol.* **9,** 592–597 (2013).